

2

# NAVAL POSTGRADUATE SCHOOL

## Monterey, California

AD-A210 657



**S** DTIC  
ELECTE  
AUG 2 1989  
B **D**

# THESIS

Analysis of Forest Fire Smoke  
Using Satellite Imagery

by

Peter J. De Vries Jr.

March 1989

Thesis Advisor: Philip A. Durkee

Approved for public release; distribution is unlimited.

Original contains color  
plates: All DTIC reproductions  
will be in black and  
white

89

156

Unclassified

security classification of this page

REPORT DOCUMENTATION PAGE

1a Report Security Classification <b>Unclassified</b>		1b Restrictive Markings	
2a Security Classification Authority		3 Distribution Availability of Report <b>Approved for public release: distribution is unlimited.</b>	
2b Declassification/Downgrading Schedule		5 Monitoring Organization Report Number(s)	
4 Performing Organization Report Number(s)		7a Name of Monitoring Organization <b>Naval Postgraduate School</b>	
6a Name of Performing Organization <b>Naval Postgraduate School</b>	6b Office Symbol <i>(if applicable)</i> <b>35</b>	7b Address (city, state, and ZIP code) <b>Monterey, CA 93943-5000</b>	
6c Address (city, state, and ZIP code) <b>Monterey, CA 93943-5000</b>		9 Procurement Instrument Identification Number	
8a Name of Funding Sponsoring Organization	8b Office Symbol <i>(if applicable)</i>	10 Source of Funding Numbers	
9c Address (city, state, and ZIP code)		Program Element No	Project No
		Task No	Work Unit Accession No
11 Title (include security classification) <b>ANALYSIS OF FOREST FIRE SMOKE USING SATELLITE IMAGERY</b>			
12 Personal Author(s) <b>Peter Joseph De Vries, Jr.</b>			
13a Type of Report <b>Master's Thesis</b>	13b Time Covered From To	14 Date of Report (year, month, day) <b>March 1989</b>	15 Page Count <b>82</b>
16 Supplementary Notes <b>The views expressed in this thesis are those of the author and do not reflect the official policy or position of the Department of Defense or the U.S. Government.</b>			
17 Cosubject Codes		18 Subject Terms (continue on reverse if necessary and identify by block number)	
Field	Group	Subgroup	<b>remote sensing, nuclear winter, forest fire smoke, nuclear warfare;</b> <i>Military Thesis (KT)</i>
19 Abstract (continue on reverse if necessary and identify by block number) <b>NOAA-9 AVHRR data from 17 and 18 September 1987 were used to perform forest fire smoke analysis and tracking. The analyses included alignment, subtraction and division of image digital values to produce an Aerosol Particle Size Index (S<sub>p</sub>) after Frost (1988). S<sub>p</sub> provides information about the slope of the aerosol particle size distribution curve and can be used to infer particle size distribution changes over time. The results provide evidence that the smoke aging process may be successfully studied using satellite imagery, provided careful analysis and removal of background effects are performed.</b>			
20 Distribution Availability of Abstract <input checked="" type="checkbox"/> unclassified unlimited <input type="checkbox"/> same as report <input type="checkbox"/> DTIC users		21 Abstract Security Classification <b>Unclassified</b>	
22a Name of Responsible Individual <b>P.A. Durkee</b>		22b Telephone (include Area code) <b>(408) 646-2044</b>	22c Office Symbol <b>63De</b>

Approved for public release: distribution is unlimited.

Analysis of Forest Fire Smoke  
Using Satellite Imagery

by

Peter Joseph De Vries Jr.  
Commander, United States Navy  
B.S., U. S. Naval Academy, 1969

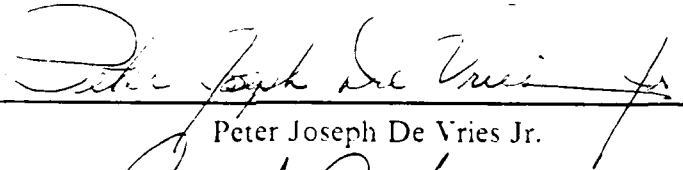
Submitted in partial fulfillment of the  
requirements for the degree of

MASTER OF SCIENCE IN METEOROLOGY AND OCEANOGRAPHY

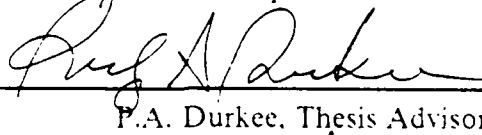
from the

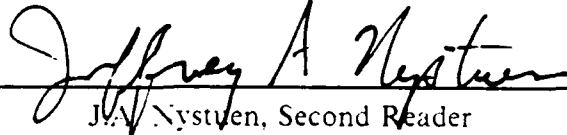
NAVAL POSTGRADUATE SCHOOL  
March 1989

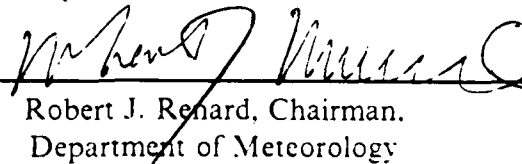
Author:

  
Peter Joseph De Vries Jr.

Approved by:

  
P.A. Durkee, Thesis Advisor

  
J.A. Nystuen, Second Reader

  
Robert J. Renard, Chairman,  
Department of Meteorology



Gordon E. Schacher,  
Dean of Science and Engineering

## ABSTRACT

NOAA-9 AVHRR data from 17 and 18 September 1987 were used to perform forest fire smoke analysis and tracking. The analyses included alignment, subtraction and division of satellite image digital values to produce an Aerosol Particle Size Index ( $S_{12}$ ) after Frost (1988).  $S_{12}$  provides information about the slope of the aerosol particle size distribution and can be used to infer particle size distribution changes over time. The results provide evidence that the smoke aging process may be successfully studied using satellite imagery, provided careful analysis and removal of background effects are performed.

Accession For	
NTIS GRA&I	<input checked="" type="checkbox"/>
DTIC TAB	<input type="checkbox"/>
Unannounced	<input type="checkbox"/>
Justification	
By _____	
Distribution/	
Availability Codes	
Dist	Avail and/or Special
A-1	



## TABLE OF CONTENTS

I. INTRODUCTION.....	1
A. MOTIVATION.....	2
B. OBJECTIVES.....	4
C. ORGANIZATION.....	4
II. THEORY.....	5
A. AEROSOLS.....	5
1. Smoke Particle Generation and Plume Content.....	6
2. Elemental Carbon.....	8
3. Aerosol Modifications.....	10
B. RADIATIVE TRANSFER THEORY.....	13
1. Scattering, Absorption and the Index of Refraction.....	13
2. Bimodal Size Distribution.....	15
3. Optical Depth.....	17
4. Scattering Regimes.....	17
5. The Radiative Transfer Equation.....	18
6. Phase Function.....	19
7. Optical Depth and Radiance.....	20
C. PRACTICAL RTE APPLICATION.....	22
D. SMOKE PLUMES AND EXPECTED EFFECTS.....	25
III. PROCEDURES.....	27
A. DATA ACQUISITION AND CORRECTION.....	27
B. DATA PROCESSING.....	29
IV. ANALYSIS.....	31
A. SYNOPTIC ANALYSIS.....	36

B.	ANALYSIS OF THE SMOKE PLUME OVER WATER.....	38
1.	Smoke Above the Ocean Surface.....	41
2.	Smoke and Surface Radiance Changes.....	42
3.	Smoke Interactions with the Stratus Deck.....	43
C.	CROSS-PLUME ANALYSIS.....	43
D.	18 SEPTEMBER, OVER WATER ANALYSIS.....	44
E.	ANALYSIS OF THE SMOKE OVER LAND.....	51
F.	UNIVERSITY OF WASHINGTON FINDINGS.....	60
V.	CONCLUSIONS AND RECOMMENDATIONS.....	64
	LIST OF REFERENCES.....	67
	INITIAL DISTRIBUTION LIST.....	70

## LIST OF TABLES

TABLE 2.1. AEROSOL CHARACTERISTICS FROM BURNING WOOD.....	9
TABLE 2.2. CHARACTERISTICS OF VEGETATION FIRES.....	9
TABLE 2.3. INDEX OF REFRACTION FOR VARYING SOOT CONTENT.....	15
TABLE 3.1. AVHRR RESPONSE WINDOWS.....	28
TABLE 3.2. REMAPPED IMAGE SCALES.....	29
TABLE 4.1. SUMMARY OF MECHANISM EFFECTS.....	35

## LIST OF FIGURES

Fig. 2.1.	Phase function diagram showing a marine aerosol compared to forest fire smoke. The phase function is plotted for smoke directly over the fire and after 44 hours have elapsed.....	21
Fig. 4.1.	Channel 1 AVHRR Image, 2310 UTC 17 September 1987: The image depicts the smoke plume off the California coast.....	32
Fig. 4.2.	A profile segment from the smoke plume that has been subjected to a five pixel running average.....	33
Fig. 4.3.	Color Enhanced $S_{12}$ Image, 17 September 1987: The locations of profiles A-H drawn for analysis are shown.....	39
Fig. 4.4.	The day 1, $L_1$ and $L_2$ values of the length-wise profiles A-D produced for analysis are shown.....	40
Fig. 4.5.	The day 1, $S_{12}$ lengthwise profiles A-D produced for analysis are shown.....	40
Fig. 4.6.	The day 1, $L_1$ and $L_2$ profiles E-H produced for analysis are shown.....	45
Fig. 4.7.	The day 1, $S_{12}$ cross-plume profiles E-H produced for analysis are shown.....	46
Fig. 4.8.	Color Enhanced $S_{12}$ Image, 2259 UTC 18 September 1987: The locations of profiles A-D drawn for analysis are shown.....	48
Fig. 4.9.	The day 2, $L_1$ and $L_2$ profiles produced for analysis are shown.....	50
Fig. 4.10.	The day 2, $S_{12}$ profiles produced for analysis are shown.....	50
Fig. 4.11.	Channel 1 AVHRR Image, 18 September 1987: The locations of profiles A-D drawn through the CA and OR fires are shown.....	53
Fig. 4.12.	The SW-NE profile (B) of the OR fire comparing the $L_1/L_2$ ratios of day 1 to day 2 is depicted.....	54
Fig. 4.13.	The W-E profile (D) of the CA fire comparing the $L_1/L_2$ ratios of day 1 to day 2 is depicted.....	54
Fig. 4.14.	Color Enhanced $L_1/L_2$ Image on day 1: The smoke plume over land is shown.....	56



- Fig. 4.15. Color Enhanced  $L_1/L_2$  Image on day 2: The smoke plume over land is shown..... 57
- Fig. 4.16. Channel 4 AVHRR Enlarged Image taken of day 1: Within the box are several darker hot spots of active combustion..... 58
- Fig. 4.17. Channel 4 AVHRR Image taken on day 2: Within the box are more intense and more numerous hot spots than on day 1..... 59
- Fig. 4.18. A comparison of the initial size distribution curve with that of 44 hours. This demonstrates the size distribution changes that take place during the aging process (University of Washington data)... 62
- Fig. 4.19. Accumulation Mode Particle Size Growth: The particle size changes are depicted for the period of the U. of W. study. The geometric volume diameter of the particles in the accumulation mode is plotted against the age of the smoke. The measurements are differentiated by the value of the light scattering coefficient due to dry particles ( $\sigma_{sp}$ ). The circles and solid line are associated with a  $\sigma_{sp}$  between  $2.0 \times 10^{-2}$  and  $5.0 \times 10^{-4}$ , the triangles and dashed line with  $\sigma_{sp}$  between  $5.0 \times 10^{-4}$  and  $1.0 \times 10^{-3}$  and the stars and dotted line with  $\sigma_{sp}$  larger than  $10^{-3}$ ..... 63

## ACKNOWLEDGMENTS

I wish to express my gratitude to Mr. Richard A. Kohrs and Mr. Craig E. Motell for their invaluable assistance throughout the project. Without their programming skills in the IDEA Lab and their unending patience with this novice and mistake-prone operator meaningful results never would have been obtained. In addition, I wish to thank Dr. Philip A. Durkee for his encouragement that the research and analysis were worthwhile and his continued assurance that "it will get finished". Lastly, I wish to thank my wife, Barbara, and son, Garth, for their patience and involvement, particularly for their patience over the final weeks of the effort when the pressure was on to finish.

## I. INTRODUCTION

The overwhelming effects of a global nuclear war are the subject of serious world-wide concern and of much study by scientists. The destruction caused by exploding nuclear weapons would be only the beginning of a long and miserable time for earth's inhabitants. The consequences of a global nuclear war are analogous to a bold theory that explains the mysterious disappearance of the dinosaurs 65 million years ago. The disappearance hypothesis says that a large meteor impacted the earth with such force that it penetrated far into the mantle (Alvarez et al., 1980). The penetration injected debris into the atmosphere and triggered a period of intense volcanism. The resulting dust and gases blocked incoming solar radiation and lowered the earth's temperature. The lowered temperature caused a severe "winter" lasting several years. The dinosaurs failed to adapt to the sudden and severe climatic change and perished.

Global nuclear war would similarly affect the atmosphere by injecting large amounts of dust into the atmosphere from ground-level explosions. Additionally, fireballs from air bursting nuclear weapons would start numerous large, uncontrollable fires that would pour dense smoke into the atmosphere (Crutzen and Birks, 1982).

Many recent studies have focused on the climatic and meteorological effects of a major nuclear conflict. Estimates of the war's effects are primarily investigated by examining natural occurrences, extrapolating or modeling those results to a larger scale and predicting climatological impact. Angell and Korshover (1985) investigated temperature changes associated with major

volcanic eruptions. Crutzen et al. (1984) estimated the atmospheric effects of the large fires a nuclear conflict would generate. Turco et al. (1983) showed that there would be large drops in earth's temperature on the continents due to sunlight reductions. Porph et al. (1986) modeled the behavior of forest fire smoke immediately after its generation. Chung and Le (1984) tracked long range transport of dust and smoke in an effort to understand particle suspension, transport and rain out. Each of the above mentioned studies contributed some additional understanding to the nuclear winter knowledge base. There are many more that are too numerous to mention.

#### **A. MOTIVATION**

While each study contributed to the understanding of how aerosols behave and the ability of aerosol to modify the earth's climate, much more remains to be discovered. An area in which more knowledge would be helpful is modification of smoke particle size distributions over time. The size distribution of aerosol particles within the atmosphere directly affects the amount of solar radiation reaching the earth's surface and the earth's temperature. The size distribution of the particles is dependent on several influences and the rate at which the influences modify the distribution is of particular interest. The restoration of normal solar heating to the earth's surface as the atmosphere is cleared of dense concentrations of aerosols would determine the length and severity of this "nuclear winter".

Additional motivation for understanding this aging process is the increasing reliance upon weapons and sensors that use portions of the electromagnetic (EM) spectrum for guidance and information collection. The continued employment of these highly technological weapons and sensors is

assured because they have become indispensable for gathering information and delivering ordnance while minimizing risk to human life. The performance of such weapons and sensors is degraded by the presence of large amounts of atmospheric aerosols. These weapons and sensors are expensive and in relatively short supply. Therefore, good management of these assets on the modern battlefield may be critical to success. The battlefield, or portions thereof, may be obscured by smoke, dust and haze that is caused by the battle itself or by other sources. The ability of the assigned environmentalist to identify weapon or sensor performance-denigrating conditions and match weapon performance criteria to the existing environment should add to battle management ability and the probability of success.

To contribute to this success the environmentalist needs valid and timely information from reliable sources. Perhaps most reliable would be remotely sensed data from sensors external to the battle problem. The Advanced Very High Resolution Radiometer (AVHRR) such as used for data in this thesis is a prime example. Its multi-channel capability can increase the knowledgeable environmentalist's available information several-fold. The information provided by such satellite imagery needs to include spatial variations in the aerosol component mixture as well as density. The components which make up the aerosol mix will vary in horizontal and vertical disbursement, varying the make-up of the particle size distribution. Weapons systems relying on different portions of the EM spectrum will suffer degradations based upon the particle size distribution of the aerosols affecting their particular operating spectrum. Therefore, the ability of the environmentalist to identify the spatial variations and predict time governed size distribution changes will directly contribute to the effective use of high technology weapons and sensors.

## **B. OBJECTIVES**

The objective of this thesis is to examine the feasibility of using satellite imagery to contribute to the battle management knowledge base in two ways. The first contribution is to examine and track the smoke from a major forest fire using satellite imagery. This is done by examining the vertical thickness and placement of the smoke, the smoke density and optical thickness, and the shape of the particle size distribution curve. These characteristics give the smoke its optical properties. Secondly, the thesis will examine how the particle size distribution curve shifts over time. The goal is to project particle size distribution shifts based on an observed shift occurring over approximately 48 hours.

## **C. ORGANIZATION**

Chapter II discusses radiative transfer theory involving atmospheric aerosols, the mechanics and characteristics of forest fire smoke and how aerosol distributions are modified over time. The data set, its acquisition and manipulation for analysis are discussed in Chapter III. Chapter IV presents an analysis of the satellite imagery, the synoptic situation and the aging process which introduces spatial variability into the aerosol mixture. Chapter V presents the conclusions and recommendations for future study.

## II. THEORY

### A. AEROSOLS

Aerosol particles in the atmosphere are formed by three processes. They result from conversion of gaseous elements to particles, suspension of particulate matter by mechanical means, or break-up of larger particles already in suspension. Within a forest fire smoke plume, conversion of produced gases and suspension of particles are the active mechanisms for aerosol formation. Each mechanism produces particles with different size characteristics. Particles produced by gaseous conversion are about one micrometer ( $\mu\text{m}$ ) in radius and smaller, whereas particles produced by mechanical means have mean radii that range between 2 and 50  $\mu\text{m}$ . We express the size in mean radius because aerosols typically have widely dispersed particle sizes within a mixture. Size distribution is an important characteristic that determines transfer of radiated and transmitted EM energy in the atmosphere.

A convenient mathematical description of the particle size distribution can be made if we assume that all particles are spherically shaped. Using this assumption, we let  $N$  be the number of particles in a given volume of air and then,

$$N = \int_0^{\infty} dN(r)/dr \, dr$$

where  $dN(r)/dr$  represents concentration of particles of a particular size and is integrated across all particle sizes. The conventional presentation of particle size distribution data is to plot  $\log dN(r)/dr$  versus  $\log r$ . The area under the

curve is proportional to the mass of the aerosol over a given size range provided that the particle concentration remains constant (Friedlander, 1977).

Several size distribution models have been developed through extensive analysis of aerosol particle sizes in specific environments. Most notable for their work in differing atmospheric conditions are Shettle and Fenn (1979). Their models for marine, rural, and urban environments provide optical properties as a function of changing relative humidity and varying particle size within the environment. While models serve as a guide, the natural variability of the atmosphere must be accounted for in dealing with specific cases. The specific effects of humidity on the optical properties of the particular distribution functions will be discussed in section II.B.3.

#### **1. Smoke Particle Generation and Plume Content**

The general characteristics of forest fire smoke are directly related to the type and amount of fuel being consumed and to the intensity of the fires.

The burning process can be conveniently differentiated into two phases: high temperature, flaming combustion during which sooty smoke is formed, and low temperature, smoldering combustion during which primarily hydrocarbons are formed. The sooty smoke is of greater significance for the atmospheric radiation balance because such smoke absorbs sunlight very effectively. Smoldering combustion on the other hand, produces an aerosol that predominantly scatters rather than absorbs sunlight. (Pitcock et al., 1986).

Aerosols in a smoke plume have particle sizes from 0.01 to 60  $\mu\text{m}$  in radius and are very effective in reducing visibility (Radke et al., 1978). The majority of the particles are in the 0.1 to 1.0  $\mu\text{m}$  range with median size about 0.6  $\mu\text{m}$ . This size is very efficient at scattering visible light (0.4-0.8  $\mu\text{m}$ ) (Waggoner et al., 1981).

Aerosol particles are generated by several processes in a forest fire. Each process produces particles with specific characteristics. The combustion



process produces many identifiable gaseous elements that are chemically or photochemically altered within the atmosphere. The reactions within the atmosphere and additional atmospheric cooling cause particles to form directly from these gaseous elements. A large proportion of aerosol particles formed under these circumstances are very small. Some of them are on the order of 100 Angstroms in size. Invariably the particles are smaller than  $0.1 \mu\text{m}$ . Production of the particles from the gas phase is called homogeneous nucleation (Friedlander, 1977). The small particle production is associated with smoldering, cooler fires. Stiles (1983) found that in a controlled environment with slow oxidation such as a wood burning stove, that 70-80% of wood burning particulate emissions were below  $1.25 \mu\text{m}$  in equivalent spherical radius.

In active combustion where flames are present, somewhat larger aerosol particles are produced by mechanical means. Gases within the fuels are rapidly expanded during combustion. This rapid expansion causes miniature explosions within the fire. The explosions throw particles into the base of the smoke plume to be carried aloft by thermal convection (Porch et al., 1986). Particles in this size range are often in the accumulation mode. Accumulation mode particles also can be produced when smaller particles collide and combine, hence the name accumulation. Accumulation mode particles range in size from  $0.1 \mu\text{m}$  to  $3.0 \mu\text{m}$  with a mean particle size of  $0.3 \mu\text{m}$ .

Mechanical scouring of the forest floor by ground-level, high speed, thermally generated winds is a third process by which aerosols are generated in forest fires. Particles as large as 1 cm in diameter can be added to the smoke plume by this mechanism. Palmer (1981) reported firestorm winds in excess of  $70 \text{ m sec}^{-1}$ , which can loft significant quantities of mineral and fire fuel residues into the atmosphere to heights of 1000 meters or more. Inclusion of these

supermicron sized particles is important to our understanding of forest fire smoke behavior. Their inclusion in the initial aerosol size distribution is important when modeling the very early optical effects close to the fire because they are very absorptive due to their large size. In addition, these large particles serve as coagulation centers for optically active, visible-wavelength, particles that are the most long lived and assist in scavenging them from the atmosphere (Porch et al., 1986).

## 2. Elemental Carbon

Another important characteristic of smoke is its graphitic or elemental carbon (EC) content. The EC (soot) content of smoke determines its absorption and is important to the extinction of EM energy. EC is formed only during flaming combustion (Crutzen et al., 1984). Normally, production of elemental carbon takes place in two size ranges. The first is the accumulation mode (radii 0.05-0.5  $\mu\text{m}$ ) and the second is the nuclei mode (radii less than 0.05  $\mu\text{m}$ )(Wolff, 1985).

Elemental carbons may make up 50% of the mass of generated aerosols in free burning fires. EC's averaged 33% in test wood fire studies found during extensive literature research (Crutzen et al., 1984). However, test fires on other vegetation types revealed that the EC production was more normally 10% of the aerosol mass. Forest fire smoke soot content depends on dryness of the fuels, the type of fuel consumed and the moisture within the environment. Nighttime burn rates are normally slower due to higher relative humidity. Tables 2.1 and 2.2 from Crutzen et al., (1984) show free burning fires produce the highest levels of elemental carbon, but smoldering fires produce the greatest percentage of aerosols to the fuel consumed.

**TABLE 2.1. AEROSOL CHARACTERISTICS FROM BURNING WOOD**

Fuel	Aerosol Yield	EC
Fireplace, Softwood	0.9 %	33 % of Aerosol
Fireplace, Hardwood	1.0 %	8 % "
Residential wood		13 % "
Test Fires		50 % "
Test Fires hardwood	.085-1.6 %	
fibreboard	.75 %	
Test Fires	1.0-2.5 % (flaming)	
	3.1-16.5 % (non-flaming)	
Test Fires	1.5 %	40 % of Aerosol
Test Fires	0.2-0.6 %	
AVERAGE	1.5 %	33 % of Aerosols

**TABLE 2.2. CHARACTERISTICS OF VEGETATION FIRES**

Fuel	Aerosol Yield	EC
Slash Burns		10 %
Vegetation		7.1 %
Forest Fire		10 %
Forest Fire	4 %	25 %
Agriculture		9.0 %
Forest Fires		
60% flaming	1 %	15 %
40% smoldering	6 %	2.5 %
Forest Fires	7 %	
Forest Fires		4.0 %
Hi-intensity FF	44 %	
Lo-intensity FF	2-4 %	
AVERAGE	6 %	10 %

The extinction coefficient of elemental carbon is very high compared to other aerosol components.

If the smoke particles are assumed to contain an amorphous elemental carbon fraction on the order of 20% and have typical dimensions on the order of 0.1  $\mu\text{m}$  to 1.0  $\mu\text{m}$ , about half the extinction events (defined as a photon interacting with a particle) for photons at visible wavelengths result in the photon being absorbed by the particle. In contrast, for dust aerosols of the same size, about 2 in 100 events result in

absorption, and for pure water less than 1 in a million result in absorption. (Pittock et al., 1986)

Soot particles may be suspended for long periods within the atmospheric system. The small particle size that inhibits sedimentation, and the hydrophobic nature of soot that inhibits condensation and rain out, contribute to the long period suspensions. Rahn et al.(1982) estimated that suspension of soot particles could last 20 days in the lower atmosphere and as much as one year in the stratosphere. In addition Chung and Le (1984) were able to observe the transport of forest fire smoke over several thousand kilometers during the 1980-1982 Canadian fire seasons.

### **3. Aerosol Modifications**

According to Friedlander (1977), there are several mechanisms that cause space and time variability of aerosol size distributions. These mechanisms include diffusion, deposition, condensation and coagulation.

Diffusion is active transport in which particulate matter is spread outward from the origin. The dilution is in response to random Brownian movement and can be expressed in terms of a coefficient of diffusion.

A second mechanism is identified as deposition, or sedimentation, defined as the removal of particles by collection on fixed surfaces through either convective or inertial processes.

A third process is that of coalescence, normally referred to as condensation. Condensation is the process by which increasing relative humidities due to changing environmental conditions will modify the optical properties of the aerosol mix (Shettle and Fenn, 1979). Condensation is important to our case study because the smoke originating over land is advected seaward and possible relative humidity changes might modify the behavior of the

smoke. Condensation depends on the hygroscopic properties of the particles generated during the combustion process and the size of the particles. Water soluble particles have an affinity for growth with increasing relative humidity, and larger particles collect water more efficiently than those that are smaller (Hanel, 1976).

The fourth and final process is coagulation. Coagulation is the most critical mechanism for the modification of the smoke size distribution. The random movement of aerosol particles within the containing volume causes collisions between particles. Coagulation takes place when particles collide and adhere to each other. Coagulation is a function of particle concentration within a volume and is highest when many particles are packed in a very small space. When the particles adhere to one another the particle volume remains constant but the surface area is reduced. This reduces particle density and changes the optical properties of the mixture.

The rate of coagulation and therefore the rate of change of the optical properties may be calculated using a method formulated by Fuchs (1964). Assuming particles adhere without rebounding, the rate of formation due to the random Brownian motion is

$$dn_k/dt = K_{ij} n_i n_j$$

and

$$K_{ij} = (r_i + r_j) (D_i + D_j) \beta_{ij}$$

for  $k = i + j$  and where  $r_i$  and  $r_j$  are initial particle radii and  $D_i$  and  $D_j$  are the

corresponding diffusion coefficients.  $\beta_{ij}$  is the slip correction term,  $K_{ij}$  is the thermal coagulation coefficient, and  $n_i$  and  $n_j$  are the respective number of particles. The diffusion coefficients are derived empirically to include the region where particle slip is important and are functions of absolute temperature, air viscosity and mean free path.  $\beta_{ij}$  is a function of the geometry of interception, the diffusion coefficients and the relative thermal velocity of the particles. Coagulation obviously causes a change in concentration within a given volume.

The thermal coagulation coefficient is made up of several other coagulation coefficients:

$$K_{ij} = K_{ij}^T + K_{ij}^S + K_{ij}^B$$

$K_{ij}^T$  is the coefficient for turbulent shear coagulation and  $K_{ij}^S$  is the sedimentation differential settling coagulation coefficient and  $K_{ij}^B$  is the Brownian coagulation coefficient. The values for  $K_{ij}^T$  and  $K_{ij}^S$  are derived from Friedlander (1965). Under normal atmospheric conditions where the concentration of large particles is low and there is little turbulence these coefficients make negligible contributions to the thermal coagulation and the Brownian coefficient is the dominant term. However, for forest fires the turbulent and settling terms are important to formation of the particle size distribution. Numerical modelling of coagulation effects on an assumed particle size distribution performed by Porch et al. (1986) showed that coagulation reduced the number of particles in a smoke plume in the 0.1 - 1.0  $\mu\text{m}$  size range. Coagulation was also shown to promote the growth of particles in the supermicron size range of up to 50  $\mu\text{m}$  in radius. The overall result was a bimodal size distribution with particle mean radius size peaks at 0.3  $\mu\text{m}$  and 5.0

or  $10.0 \mu\text{m}$ . This bimodal distribution for smoke is consistent with Shettle and Fenn (1979). Their urban aerosol mixture composed of smoke and rural aerosols was also bimodal in structure. Empirical instrument measurements (Wallace and Chaun, 1976) showed a large particle mass-median radius of about  $2.0\text{-}4.8 \mu\text{m}$  for California brush fires. This agrees with actual fire research by Fosberg and Record (1980). The resulting bimodal distribution of particle sizes evolves over time. Typically the largest particles settle out of the smoke plume once the turbulent energy of the firestorm is dissipated (Porch et al., 1986). The settling of the largest particles occurs in the first hour after the smoke clears the firestorm. At the end of the first hour the particle size distribution typically shows one mode with a mean size of about  $0.6 \mu\text{m}$ . From this point, the remaining particles shift toward a larger mean particle size due to coagulation. The effect of this size distribution shift on the optical properties and the effect on remotely sensed values will be discussed in section II.D and the introductory paragraph of Chapter IV.

## **B. RADIATIVE TRANSFER THEORY**

The introduction of aerosols into a clean atmosphere causes scattering or absorption of EM energy in all frequencies, including those of visible light and infrared radiation. The light scattering properties of aerosols are very useful in the study of the aerosols themselves. By observing the behavior of light in the presence of aerosols, information can be obtained about the particle size distributions.

### **1. Scattering, Absorption and the Index of Refraction**

Scattering of energy by an individual particle has been shown to depend on the size, refractive index and shape of the particle as well as the

wavelength of the incident EM wave (van de Hulst, 1957). In essence only two reactions can take place when transmitted EM energy encounters an aerosol particle in the atmosphere. The energy can be either redirected by the particle in the scattering process or be absorbed. During the absorption process energy is received and changes the state of the particle. Larger size particles in the smoke plume and elemental carbons are particularly efficient at absorption, while smaller sized particles are better at scattering.

The index of refraction, represented by

$$m = n + i\nu,$$

is a mathematical expression of the scattering and absorptive properties of particles. The amount of scattering that takes place in an aerosol is partially controlled by the complex index of refraction,  $m$ . The real part of this complex number,  $n$ , is a ratio of the speed of light in one substance to another. The imaginary part,  $i\nu$ , indicates the potential for particle absorptivity. The absorptivity is closely related to wavelength, but is generally less than  $10^{-2}$  where wavelengths are less than  $3 \mu\text{m}$  for aerosol regimes with large particles (Shettle and Fenn, 1979).

Indices of refraction for particulate mixture models which are regionally dependent were developed by Shettle and Fenn (1979). The models developed include marine aerosols, urban aerosols and rural aerosols. The optical properties of extinction, scattering, absorption and single scatter albedo are derived for various wavelengths of radiation under changing conditions of relative humidity. Single scattering albedo is expression for the ratio of scattering to extinction for a certain aerosol mixture. It is conventionally



represented by  $\omega_o$ . In addition to optical properties of the mixture, Shettle and Fenn (1979) provide the refractive indices of the constituent particles. In order to accurately describe the make up of the smoke plume's particle size distribution we must determine the proper index of refraction. This index will directly effect the optical depth of the aerosol concentration within the atmosphere.

Shettle and Fenn (1979) used a mixture of 80% rural aerosols and 20% sootlike particles to model urban aerosols. Following their procedure, but incorporating various soot levels for mixtures we can expect to encounter in this study, Table 2.3 was produced.

**TABLE 2.3. INDEX OF REFRACTION FOR VARYING SOOT CONTENT**

Mixture	% Carbon	Index of Refraction
Shettle & Fenn	20 %	1.55 - 0.0048 i
Smoke # 1	33 %	1.59 - 0.17 i
Smoke # 2	50 %	1.64 - 0.25 i
Soot	100 %	1.75 - 0.43 i

## 2. Bimodal Size Distribution

Shettle and Fenn (1979) shows the urban aerosol mixture having two modes of particle size concentrations. These modes are centered at radii of 0.03  $\mu\text{m}$  and 0.5  $\mu\text{m}$ . The normalized standard deviations of the particle sizes from those centers are given as 0.35 and 0.40 respectively. A similar bimodal distribution was assumed by Porch et al. (1986), based on laboratory experiments. The two particle size peaks are at 0.5  $\mu\text{m}$  and 5.0  $\mu\text{m}$  with normalized standard deviations of 1.75 and 1.70 respectively. The forest fire smoke has more widely dispersed size variations and the peaks in the distribution are more widely separated. The spread is due to the numerous

processes responsible for aerosol production in a fire. Porch et al. (1986) also used a derived index of refraction of  $1.53 - 0.05i$  which is higher in both terms than the Shettle and Fenn (1979) urban aerosol model. The effect of the higher index of refraction with its much higher absorptivity index is two-fold. Primarily it increases the total extinction, increasing the optical depth. When the optical depth shuts off all radiation from the surface, we are unable to 'see' through the smoke and the radiance received at the satellite is totally dependent upon the particles within the smoke plume. The second effect is to shift the peak of the small particle (submicron) optical effects to smaller particles making it appear as though the particles in the mixture are smaller than they are (Porch et al., 1986).

In order to calculate the overall effect of many particles we multiply the extinction or scattering efficiency by the particle cross-sectional area and the size distribution of the particles within the atmospheric system.

Scattering by the aerosol is described by the scattering coefficient

$$\sigma_{\text{scat}} = \int_0^{\infty} \pi r^2 Q_{\text{scat}} dN(r)/dr dr$$

and the extinction of the aerosols is given similarly by

$$\sigma_{\text{ext}} = \int_0^{\infty} \pi r^2 Q_{\text{ext}} dN(r)/dr dr.$$

$Q_{\text{scat}}$  and  $Q_{\text{ext}}$  are the scattering and extinction efficiencies derived above for a particle with radius  $r$  and complex index of refraction  $m = n + i\nu$ .  $dN(r)/dr$  describes the size distribution of the particles.

### 3. Optical Depth

The quantity that describes the concentration of aerosols in the vertical column of the atmosphere is the optical depth. Optical depth is defined as

$$\delta = \int^H \sigma_{\text{ext}} dz.$$

The optical depth is dependent upon the magnitude of the extinction coefficient and indicates the amount of radiation that passes through the atmosphere. The limits of integration represent the total depth of the atmosphere which contains the aerosol.

### 4. Scattering Regimes

Another important aspect to the amount of visible and near-infrared radiation passing through an aerosol field and reaching a sensor is the relationship of particle size to wavelength. The size index,  $S$ , is defined as

$$S = 2\pi r/\lambda.$$

The interactions between visible and near-infrared EM radiation and aerosol particles is dependent upon this size index. This relationship can be divided into three regimes in which the interaction of the energy with the particle is governed by different laws.

When  $s \ll 1$  the visible and near-infrared scattering taking place is the result of molecules in the atmosphere and is governed by Rayleigh theory. This molecular scattering makes a significant contribution to the overall effect of the atmosphere. However, the contribution is relatively uniform horizontally

and will be relegated to the role of "background aerosol" in the discussion presented here. This background aerosol will be removed from imagery to enable a full concentration on the smoke plume.

In cases where  $s \approx 1$ , the visible and near-infrared energy scattering is due to the presence of aerosols within the atmospheric system. Mie theory describes aerosol interaction and scattering. The scattering directly affects the radiation field and is used to infer the particle distributions.

Where  $s \gg 1$ , which will certainly happen where supermicron particles have been mechanically lofted into the atmosphere, a large particle removes twice the amount of light intercepted by its cross-sectional area (van de Hulst, 1957). This is important to our understanding of particle sizes within the smoke plume and the extinction over the fire itself. The absorption of incoming solar radiation by these large particles is particularly important in their contribution to the nuclear winter hypothesis.

### 5. The Radiative Transfer Equation

It is possible to estimate the influence that particle size, types of particles and index of refraction have on energy transmitted through an aerosol field. The radiative transfer equation is used to investigate these influences. The equation for radiative transfer is

$$L_A(\lambda, \theta, \phi) = L_o(\lambda, \theta, \phi) e^{-\delta(\lambda)/\cos \theta} + \int_0^{\delta(\lambda)} J(\lambda, z, \theta, \phi) / \sigma_{ext}(\lambda, z) e^{-\delta(z\lambda)/\cos \theta} d\delta / \cos \theta,$$

where

$L_A(\lambda, \theta, \phi)$  = the spectral radiance,  
 $(\theta, \phi)$  = spherical coordinate angles,

$J(\lambda, z, \theta, \phi)$	= the atmospheric radiance due to scattering,
$\delta$	= the optical depth of the atmosphere,
$z$	= height in the atmosphere,
$\sigma_{\text{ext}}$	= the coefficient of extinction,
$\lambda$	= the wavelength and
$e^{-\delta(\lambda)/\cos \theta}$	= the transmittance.

The radiative transfer equation has two components. The first term represents the originating surface radiance multiplied by the direct transmittance of the atmosphere. The second term is the path added radiance source value at each position within the atmosphere multiplied by the integral of the transmittance from the position to the top of the atmosphere.

When the atmosphere is optically thin,  $\delta \ll 0.1$ , transmittance = 90% or more and single scattering predominates. In the regime where  $0.1 < \delta < 0.3$  some multiple scattering occurs and the RTE solution becomes more complex. When  $\delta$  is above 0.3 multiple scattering is dominant. This makes term two very complicated as energy is coming from all directions and the RTE solution becomes unmanageable. The increased scattering decreases the transmitted energy, eventually eliminating all surface reflectance.

## 6. Phase Function

When particles scatter radiance it exits the scattering volume at various angle. Part is scattered into the direction of the original propagation; this is forward scatter. Part is scattered back toward the source; this is back scatter. The directional distribution of the scattered energy may be plotted for a given scattering cross-section and is related to  $\sigma_{\text{scat}}$  through the scattering phase function  $P(\Theta)$ , where  $\Theta$  is the scattering angle.

This phase function specifies the fraction of radiation scattered in a certain direction. The phase function plays a large role in the radiance observed by a satellite because the geometry of the phase function varies from pixel-to-pixel within an image.

A typical integrated phase function diagram is shown in Fig. 2.1. The diagram depicts the phase function values for a typical marine aerosol versus the sampled smoke particle size distribution over the top of the OR fire and the particle size distribution of smoke after 44 hours.

A marine aerosol mixture with 80% relative humidity, index of refraction of  $1.35 - i 1.53 \times 10^{-9}$  and single scatter albedo of 0.99 is plotted versus two forest fire smoke mixtures. The forest fire smoke has a much larger index of refraction and a single scatter albedo of 0.55. The smoke exhibits more absorption and less scattering. The two smoke lines are plotted to depict the difference between the initial size distribution and the distribution after the maximum aging time available in this study. Higher values indicate the greater probability that energy will be scattered in a particular direction. As a result, larger particles in the early plume show more forward scattering than the smoke after 44 hours.

## **7. Optical Depth and Radiance**

The optical depth is related to the radiance in a linear fashion when the optical depth is less than 0.3 (Durkee, 1984). Increases in optical depth will result in more radiance observed at the satellite because of increased scattering of direct sunlight. Because optical depth is the vertical integration of extinction, the areas of an image which appear brightest are the areas of highest extinction when over a non radiating surface such as the ocean.

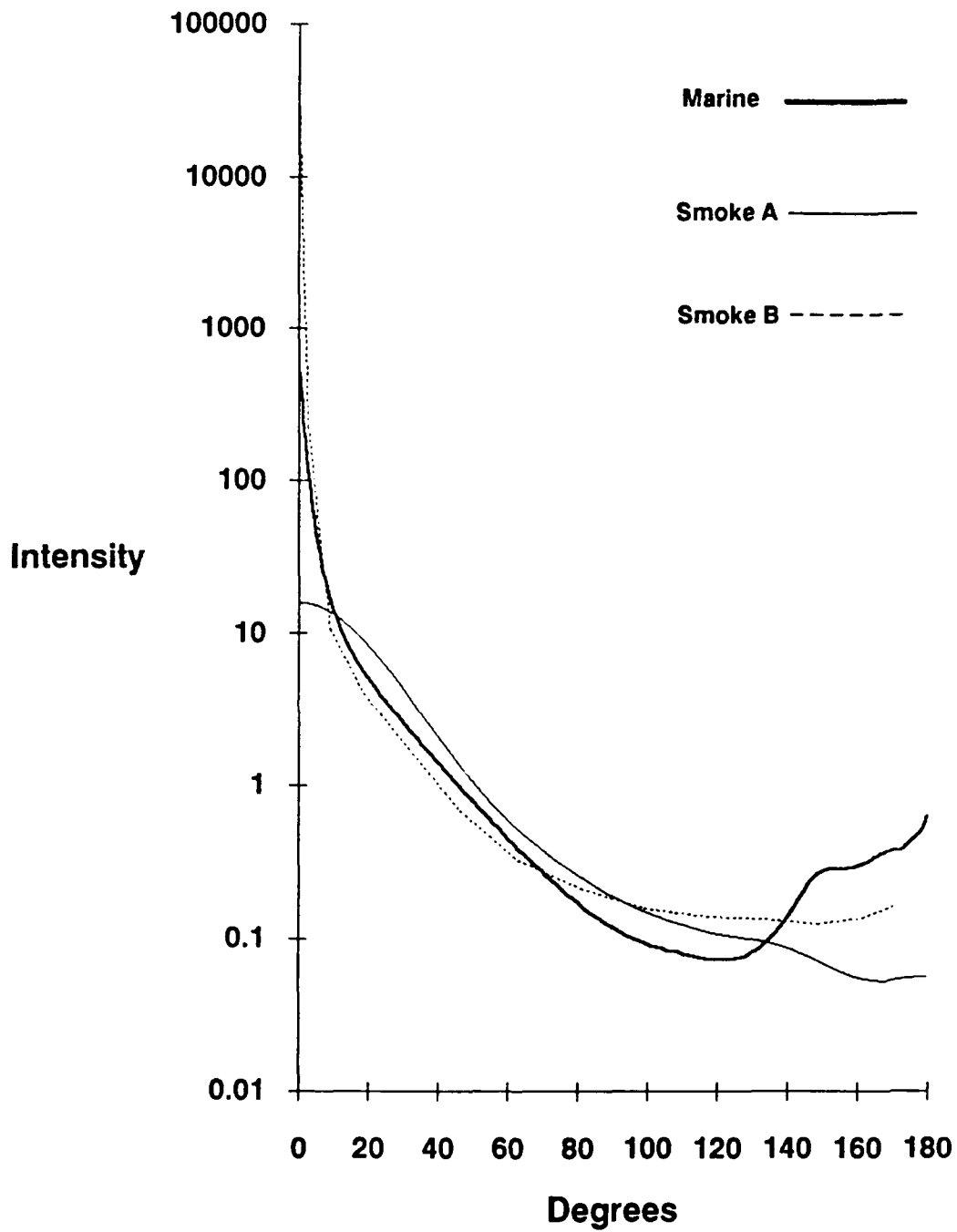


**Fig. 2.1. Phase function diagram showing a marine aerosol compared to forest fire smoke. The phase function is plotted for smoke directly over the fire and after 44 hours have elapsed.**

Increases in extinction can be related to one of three changes to the aerosol mixture: greater concentration of particles of the same size in a given volume, increase in the particle size and a greater depth of the atmosphere over which a fixed concentration is allowed to interact. In the case study in this thesis the smoke plume is capped by an inversion which limits its vertical extent. The particle concentration is fixed upon departure from the scene of the fire, assuming the smoke has undergone the modifications of the first hour. Therefore, the dominant effect is a change in particle size.

As a dry particle size distribution shifts upward mean particle size increases and the number of small particles decreases due to coagulation. This should decrease the optical depth in visible wavelengths and possibly decrease it in near-infrared wavelengths. The single scattering albedo should decrease as well, because fewer particles offer less surface for scattering encounters.

For particle mean size increases caused by relative humidity increases the optical depths in visible and near-infrared wavelengths will increase. Water, an efficient energy scatterer, is condensing on the smoke particles, increasing the optical depth. The increased optical depth will tend to equalize the ratio between the two wavelengths.

### **C. PRACTICAL RTE APPLICATION**

The theoretical RTE terms are readily identified as components that contribute to the radiance observed by a satellite. The terms within the RTE are dependent upon wavelength, viewing angles and aerosol size distribution. The wavelengths that are used with the smoke plume particle size distributions correspond to channel 1 and channel 2 of the NOAA-9 Advanced Very High



Resolution Radiometer (AVHRR). The channels are centered at 0.63  $\mu\text{m}$  and 0.86  $\mu\text{m}$  respectively.

The disbursement of small and large particles within the particle size distribution can be obtained by using the RTE. The aerosol dependent terms of the RTE are larger in channel 1 than in channel 2 for particle size distributions with relatively small mean particle sizes.

Frost (1988) demonstrated that a ratio between channel 1 and channel 2 ( $S_{12}$ ) can be used to indicate the slope of the particle size distribution curve. The ratio of the extinction or optical depth is directly proportional to radiance seen by the satellite over nonradiating surfaces. The aerosol-generated radiance,  $L_A$ , is proportional to the optical depth,  $\delta$ , in each channel. The ratio is expressed:

$$S_{12} = \frac{(L_A)_{0.63 \mu\text{m}}}{(L_A)_{0.86 \mu\text{m}}} \approx \frac{(\delta)_{0.63 \mu\text{m}}}{(\delta)_{0.86 \mu\text{m}}}$$

Where  $S_{12}$  is larger, small particles predominate, where it is small the large particles are dominant.

The  $L_A$  values viewed by the satellite include contributions from various components within the earth/atmosphere system. After Gordon (1978) and Durkee (1984), the radiance at the satellite ( $L_S$ ) can be approximated as the sum of several independent terms:

$$L_S = (L_G + L_W)t + L_R + L_A, \text{ over water}$$

and

$$L_S = (L_B)t + L_R + L_A, \text{ over land,}$$

where  $L_W$  is the radiance of the ocean surface which is not caused by direct reflection.  $L_G$  is specular reflectance or glitter. Both  $L_W$  and  $L_G$  are subject to atmospheric transmittance, where  $t = e^{-\delta}$  and  $\delta$  is the optical depth.  $L_R$  is the Rayleigh scattering by atmospheric molecules which is added into the radiation path to the satellite.  $L_B$  is the background radiance over land due to reflectance by vegetation and terrain.  $L_A$  is the path added radiance due to the scattering by the smoke and other pollutants in the atmosphere.  $L_A$  is the term needed for analysis.

To isolate  $L_G$  over water we select a satellite pass, or an area within a pass where the sun-satellite geometry minimizes or eliminates reflection from the water. This reduces  $L_G$  to zero. Next, from Ramsey (1968), it is assumed ocean albedo in channel 1 and channel 2 will not contribute to radiance ( $L_W \approx \text{zero}$ ).  $L_R$ , the Rayleigh scattering term, is assumed to be horizontally equal based on a relatively constant gaseous composition of the atmosphere. Rayleigh scatter effect is higher for shorter wavelengths and therefore its removal has a greater effect on channel 1 radiance. The removal has the effect of lowering the ratio between channel 1 and channel 2 radiances over a wide area (Durkee, 1984). The transmittance of the atmosphere,  $t$ , includes the absorption of radiance by the ozone layer at the top of the atmosphere. The ozone absorbs more visible radiance than infrared radiance. The unequal absorption is incorporated into the ratio through the transmittance. The ozone adjustment to the radiance values increases the ratio between channel 1 and channel 2 higher than it was before removal of the Rayleigh effect. The sum of the above corrections and adjustments is to equate  $L_S$  to  $L_A$ .

To isolate  $L_A$  over land we select two images from the same channel. One image must be free of the pollution episode of interest and must closely approximate the sun-satellite-terrain geometry that is used for the second image. The second image includes the smoke or other pollutants. The close sun-satellite-terrain geometry approximation is necessary because the first image is subtracted from the second image to eliminate background noise. Changes in season or foliage will take place if the satellite images are too many days apart, introducing inaccuracies into the process. Additionally, the satellite observation direction should be within a few degrees to account for the anisotropy of the terrain reflectance. Subtraction of the images eliminates  $L_B$  from the above equation, however it potentially introduces errors caused by radiance changes between satellite passes. The same rationale regarding Rayleigh and ozone effects can be applied to adjust  $L_S$  to arrive at  $L_A$  for the over land case.

#### **D. SMOKE PLUMES AND EXPECTED EFFECTS**

It is clear from our discussion thus far that the optical characteristics of smoke are considerably different than those of the marine aerosols discussed by Shettle and Fenn (1979) and Durkee (1984).

Smoke, having a different index of refraction with a much greater indicator of absorptivity can be expected to have a much higher optical depth for the same particle concentration. Porch et al. (1986) reported optical depths in the range of 1 - 1400. A second difference we might expect is that there will be a much wider distribution of the particle sizes within the aerosol mixture. Porch et al. (1986) worked almost exclusively with a bimodal distribution with respective peaks at 0.045 and 5.0  $\mu\text{m}$  and normalized standard deviations of 1.75 and 1.70. Taking the adjusted indices of refraction in section B.1 of this chapter and the

size distributions modeled by Porch et al. (1986) it is possible to estimate the characteristics of the smoke. A Mie scattering program can provide the extinction, absorption and single scattering albedo for both wavelengths used in this study. The computed extinction coefficients are particularly important, because the radiance viewed at the satellite in each channel is directly related to optical depth. Optical depth is the vertical integration of the extinction coefficients over the depth of the aerosol cloud. Therefore, the ratio of the extinction coefficients computed should be the same ratio as the radiance viewed at the satellite. This ratio will change as the particle size distribution changes over time based on the coagulation taking place within the plume.

These changes are observable without the sophistication of multi-channel satellite imagery. The sun is seen as red or orange when viewed through fresh smoke plumes because the small particles initially formed are more effective at scattering shorter wavelengths (blue light). As the smoke ages through the coagulation process the particles grow in size and become more effective at scattering light in all visible wavelengths. Thus the sun will appear white or light gray depending on the optical depth of the smoke. Carried to an extreme a strong concentration of large particles would be effective at scattering the longer, red wavelengths of light and the sun and moon would appear bluish when viewed through the plume. The sun and the moon were both observed to be bluish in color in connection with Canadian forest fires (Wexler, 1950).

### III. PROCEDURES

This brief section will discuss the data acquisition and manipulations used to produce the images for analysis in the next chapter. Synoptic information used in the aging process analysis was available in the Naval Postgraduate School archives, therefore no discussion is presented in this chapter.

#### A. DATA ACQUISITION AND CORRECTION

Satellite-gathered Advanced Very High Resolution Radiometer data from NOAA-9 were used for this forest fire smoke study. The NOAA-9 satellite is a sun-synchronous polar orbiting satellite which completes fourteen revolutions daily in a orbit inclined 99 degrees to the equator. It crosses the equator southbound about 0200 Local Solar Time (LST) and northbound about 1400 LST. The nominal altitude is 850 km with a spatial resolution of 1 km. The AVHRR sensor measures upwelled radiance in five narrow bands or channels of the EM spectrum, and records the data as ten bits of digital information. This provides a range of 1024 radiometric values. The viewing angle of the satellite is approximately 55 degrees in width, containing information in 2048 individual pixels. The data are transmitted as High Resolution Picture Transmission (HRPT) and recorded on magnetic tape. The data used were acquired from Scripps Institution of Oceanography, La Jolla, CA. The five channels of the sensor are responsive as shown in Tab. 3.1.

Data consisting of northbound NOAA-9 passes on 17 September (day 1), 18 September (day 2), and 28 August (clear day) 1987, showing the west coast of North America and the eastern North Pacific Ocean, are presented in this

study. The visual images from 17 and 18 September show a vigorous multi-center

**TABLE 3.1. AVHRR RESPONSE WINDOWS**

Channel No.	Bandwidth ( $\mu\text{m}$ )	Spectral Region
1	0.58 - 0.68	Red visible
2	0.72 - 1.10	Near Infrared
3	3.55 - 3.93	Mid Infrared
4	10.5 - 11.3	Thermal Infrared
5	11.5 - 12.5	Thermal Infrared

forest fire burning in the Klamath National Forest on the California-Oregon border. The northern fire center will be referred to as the OR fire and the southern fire center will be the CA fire. The data of 28 August were selected for use as background aerosol information. The satellite pass of the 28th was virtually free of clouds and evidence of major pollutants over the land mass.

To accurately subtract the background aerosol and terrain related radiance, the sun-satellite geometry of the two images must be similar. The geometry depends on the time of day and the season of the year. The change of background radiance between the August and September data required correction to properly diagnose the smoke. This correction was performed by taking three horizontal profiles in clear areas on day 1, day 2, and clear day images in channel 1 and channel 2. These profiles were analyzed to determine the value changes due to temporal and geometric differences. A correction was then applied to day 1 and day 2 images in each channel before the ratio of the channels ( $L_1/L_2$ ) was mathematically performed. The resulting ratio images were then color enhanced to facilitate interpretation of the results.

## B. DATA PROCESSING

The acquired data were processed at the Interactive Digital Environmental Analysis Laboratory (IDEA LAB) located at the Naval Postgraduate School (NPS), Monterey, CA. The VAX 8250 computer with multi-capable graphics/video displays was used to manipulate and analyze the data. The first data processing step was to remap the data onto identical coordinate projections, thereby aligning the pixels from the three days and enabling the values to be mathematically manipulated. Two sizes of images were produced (Table 3.2), each designed for a different purpose.

TABLE 3.2. REMAPPED IMAGE SCALES

Size	N/S Limits	E/W Limits	km <sup>2</sup>	Pixel Size (km)
A	40.0-44N	122-124.5W	58,548	0.91
B	36.5-43N	122-128.5W	396,000	1.42

The larger B size images show wider coverage of the smoke over the North Pacific Ocean and the A size images give a more detailed picture of the plume over land. Images were produced in individual channels 1, 2 and 4 and by dividing channel 1 values by channel 2 values to produce  $L_1/L_2$  values. Additional ratio images were made which were corrected by removal of Rayleigh scattered radiance and the effect of ozone absorption ( $S_{12}$ ). The assumption is made that the atmospheric components are uniformly distributed horizontally and, therefore, Rayleigh scatter and ozone absorption effects are compensated for everywhere equally. The algorithm also adjusts for the geometry between the sun and the satellite which varies across the image.

As previously discussed, the physical values from the satellite ranged from 0 - 1023. The satellite measured values are displayed on the CRT as 256 gray

shades and it is a relatively simple process to convert brightness counts to radiance values for channel 1 and channel 2 of the AVHRR (Kidwell, 1986). Once converted, these radiance values were used to produce a separate set of images for over-land analysis.

The clear channel 1 and channel 2 images were brighter than the respective images for both smoke days. The average difference between the images was derived for each channel. The difference was approximately 10 for channel 1 and 28 for channel 2. This average difference was added to the remainders when the clear images were subtracted from the smoke images. By adding this step we insure that the brighter clear images do not dominate the ratio formed when we divide the channel 1 corrected image by the channel 2 corrected image.



#### IV. ANALYSIS

Analysis of the data is divided into four separate sections. The first section presents the results of the synoptic meteorological analysis, estimating smoke age in various segments of the profiles and drawing inferences for size distribution changes. The second section addresses the trends of the  $S_{12}$  ratio as the smoke diffuses southward over the North Pacific Ocean. It includes abbreviated analysis of the individual contributions of channel 1 and channel 2 ( $L_1$  and  $L_2$ ) radiances, and how they affect the  $S_{12}$  values. The third section is a similar analysis performed over land. The fourth section compares these results with a similar study, using aircraft collected data, conducted by the University of Washington.

The CA and OR fires of 17 September 1987 produced large amounts of dense smoke that drifted southwest over the North Pacific Ocean. The satellite photo in Fig. 4.1 is a channel 1 image of the smoke plume on the 17th (day 1). The smoke trails off the coast and is visible in the image for about 700 kilometers, or until it reaches the latitude of San Francisco Bay, where it overrides a low lying stratus layer.

Profiles were produced of the pixel values in various transects both along and across the smoke plume for this image and images in other channels on other days. Fig. 4.2 is a typical profile. This sample profile has been smoothed by taking a five pixel running average of the values. Other profiles will be treated the same. In spite of the averaging, the profile in Fig. 4.2 still contains noise which may interfere with analysis of the trends present.



**Fig. 4.1. Channel 1 AVHRR Image, 2310 UTC 17 September 1987:  
The image depicts the smoke plume off the California coast.**

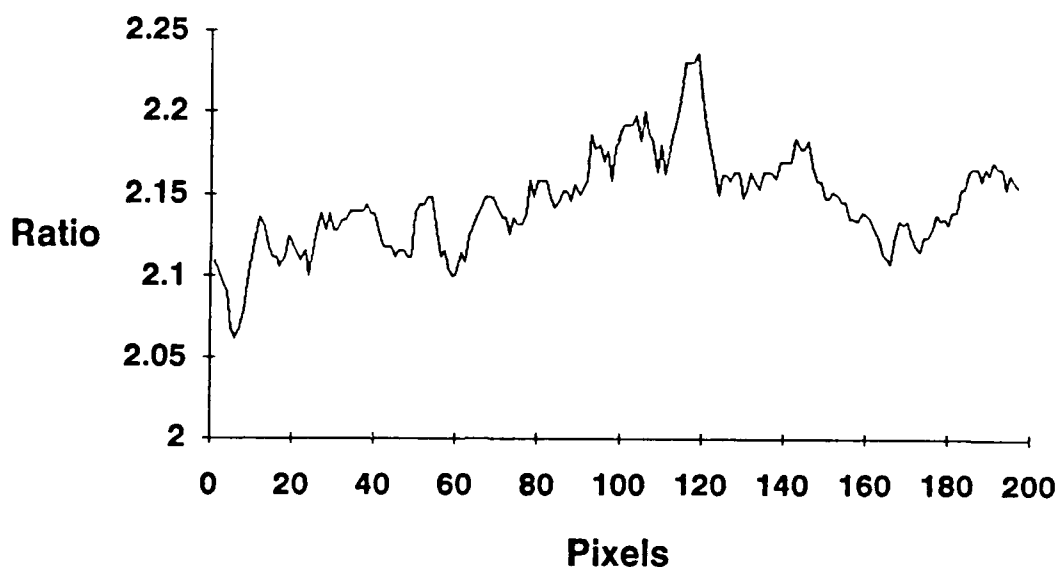


**Fig. 4.2.** A profile segment from the smoke plume that has been subjected to a five pixel running average.

There are three reasons the data exhibit this variability and two of those reasons contribute to the noisiness and the spikes.

The primary reason for the variability originates from the smoke distribution. Studies have shown that the smoke produced by the forest fire is variable in aerosol content, particle size distribution, and concentration. These variables are a function of the fuel being consumed, the intensity of the fire, the terrain involved and the meteorological contribution to plume dilution and diffusion. Particularly noteworthy are the hour to hour variations in the intensity of forest fires. Typically the higher humidity and lower temperatures associated with nighttime allow forest fighters to gain an upper hand during those hours. The smoke produced during the night could be expected to contain a higher percentage of aerosols to fuel consumed and to contain fewer carbon particles.

A second source of noisiness is geographic remapping of images in which there is a possibility that the pixels in successive images may be slightly misaligned. This error source is most important in the analysis of the smoke plume over land, in which four images are combined to produce one image for analysis.

Thirdly, the Rayleigh and ozone adjusted profiles are produced by mathematically subtracting large values and dividing the remainders. Although Rayleigh and ozone effects are nearly uniform horizontally some variations may be enhanced by the mathematics.

Porch et al. (1986) modeled the particle size distribution change for a general forest fire case over the first hour. The model indicated that the mean size of the small particles increased due to coagulation and the larger particles decreased in number due to sedimentation. Extrapolating these findings to the present case and assuming the passage of one hour, smoke should emerge from the plume above the firestorm having an initial  $S_{12}$  value. That value should show a steady decrease as the smoke diffuses outward in time and space. This generally is the case, however, greater variability in the  $S_{12}$  values is found due to other processes such as gas-to-particle conversion and condensation taking place within the plume. Examining  $L_1$  and  $L_2$  variations in relation to  $S_{12}$  changes can help identify these processes. Table 4.1 summarizes the effects of these mechanisms.

If  $S_{12}$  is increasing where  $L_1$  increases and  $L_2$  increases less or remains constant, the increase in  $S_{12}$  is consistent with gas-to-particle conversion. This is evidenced by increasing radiance in  $L_1$  from the newly formed particles, while  $L_2$  is largely unaffected. If  $L_1$  remains constant and  $L_2$  is decreasing, then less radiance scattered by the larger particles indicates gravitational settling from the

**TABLE 4.1. SUMMARY OF MECHANISM EFFECTS**

Process	$S_{12}$	$L_1$	$L_2$
Coagulation	dn	same or down	up
Condensation	dn	up	more
Sedimentation	up	down	dn more
Conversion	up	more	up
Sed. & Conv.	up	up	dn
Coag. & Cond.	dn	dn	up
Sed. & Coag.	up or dn	dn more	dn

aerosol mixture. Under these circumstances it is possible that the larger particles are also coagulating, forming larger particles heavy enough to accelerate sedimentation and decrease scattering in  $L_2$ .

If  $S_{12}$  is decreasing, a similar analysis can be conducted. If the  $L_1$  value remains constant and  $L_2$  increases, the most likely cause is coagulation. Coagulation could also be accompanied by a decrease in optical depths because the particles retain their original mass while surface area decreases. This effect depends on the size of the particles that are coagulating. The overall particle concentration decreases as well. If  $L_1$  remains constant or decreases and  $L_2$  increases it would appear as though the total number of particles per unit volume is remaining nearly constant and the mean particle size is increasing. This is an indication of water condensation on each particle. There is a possibility condensation would occur in the smoke over the North Pacific Ocean. The smoke was trapped just above the boundary layer and was close to an area of generally high humidity.

There is a probability that coagulation and sedimentation would occur simultaneously in the aging process. If this were to occur the  $L_1$  values would

decrease due to the coagulation and the  $L_2$  values would decrease due to sedimentation of the larger particles. The effect of the simultaneous  $L_1$  and  $L_2$  decrease on  $S_{12}$  would depend upon the rate of decrease. The normal result would be an increase in  $S_{12}$  because the decreasing  $L_2$  is in the denominator and has a greater effect on the ratio.

#### **A. SYNOPTIC ANALYSIS**

Accurate smoke analysis at a geographic position where the smoke is measured requires a procedure to identify the smoke and determine its age. A time-speed-distance conversion can be accomplished by using geostrophic winds at the smoke level divided by the measured distance from the fire. Analysis also requires an estimate of the environmental effects on the particles within the plume.

The height of the smoke was established through analysis of the terrain from a topographic map and matching contours to the smoke patterns. This analysis showed the smoke to be flowing downhill and following the valleys. The shape of the smoke on day 1 in channel 1 imagery was limited in its northward travel by 3000 ft contours north of each fire center. A discussion between the author and firefighting personnel confirmed that camps for fire fighters are routinely established on high ridges to escape the heavy smoke pall. Porph et al. (1989) conducted studies on the waterfall effects of smoke plume in rugged terrain and verified this finding.

Meteorological data from 0000 UTC 17 September 1987 through 0000 UTC 19 September 1987 was retrieved from the NPS archives. These data included Oakland, CA and Medford, OR soundings and 850 mb, 500 mb, and sea level pressure charts. Medford, OR, located at 42.37N and 122.87W, is the

closest meteorological station that takes regular atmospheric soundings. The Medford sounding of 1200 UTC (0400 local time) 17 September 1987 at indicated that the 896 mb pressure level was at 3000 ft, 875 mb was the top of the boundary layer and 850 mb corresponded to 1510 m. There is strong correlation between the winds from this sounding, the 850 mb contour charts and the smoke drift pattern observed in the satellite imagery. By the mid-afternoon image time the inversion was at 704 mb.

The synoptic picture analyzed from the Medford soundings and the contour charts is very stable with light northeasterly winds below 820 mb and westerlies above 700 mb. Temperature and dew point analyses indicate a strong nighttime inversion at the top of the boundary layer. Relative humidities ranged from a nighttime high of about 65% at 0400 local time, to a daytime low of 15% at 1600 local time. The synoptic stability provided a unique opportunity to analyze the smoke plume because the smoke was trapped below 1500 meters and the light winds provided minimal dilution. These conditions enhanced satellite tracking and analysis of the plume over a long distance, and also the aircraft sampling of the plume contents by the University of Washington.

The extent the plume could be analyzed using satellite imagery was limited by a layer of low altitude stratus clouds at a latitude equal to that of San Francisco. The Oakland, CA soundings indicate this layer was below 600 meters at all times. The radiance from the clouds was far brighter than the radiance of the smoke making the smoke impossible to distinguish above the layer.

The synoptic situation remained stable on 18 September 1987. However, there were some noteworthy changes in the smoke plume. By the 18th the ground-level firestorm was strong enough to cause the plume to penetrate through a weakened daytime inversion. The smoke reached at least the 700 mb

level in the atmosphere where the wind was 18 knots out of the WSW. Smoke drift to the ENE can be detected in the imagery. In addition, the typical eastern North Pacific boundary layer stratus deck had migrated further north during the night and was obscuring the surface of the ocean. The cloud deck hampered the ability to obtain  $S_{12}$  values over the water on 18 September, except for a thin sliver of smoke on the western edge of the stratus.

## **B. ANALYSIS OF THE SMOKE PLUME OVER WATER**

The profiles (A through H) produced from satellite imagery of channel 1 ( $L_1$ ) and channel 2 ( $L_2$ ) and the  $S_{12}$  ratio corrected for Rayleigh radiance and ozone absorption based on day 1 of the satellite pass are shown in Fig. 4.3. The profiles were averaged over five adjacent pixels. Profiles A-D are continuous from across the head of the fire to the southernmost extent of the plume (segments B and C are not labeled in the image). Profile A will be discussed in the next section in conjunction with other over-land data. Periodic cross-stream profiles (E through H) were produced to examine the west-to-east plume variability and demonstrate spatial variation of the maximum values across the plume. Channels 1 and 2 contribute unevenly to  $S_{12}$  over the spatial area of the smoke plume. Therefore, a simultaneous analysis (using Figs. 4.4 and 4.5) of the inter-relationship between channels 1 and 2 and the  $S_{12}$  ratio will be applied to interpret the mechanisms taking place within the plume. The point at which the cross-plume profiles were produced is shown on both figures. The zero kilometer point was chosen at the middle of the OR fire to facilitate age determination.





Fig. 4.3. Color Enhanced  $S_{12}$  Image, 17 September 1987: The locations of profiles A-H drawn for analysis are shown.

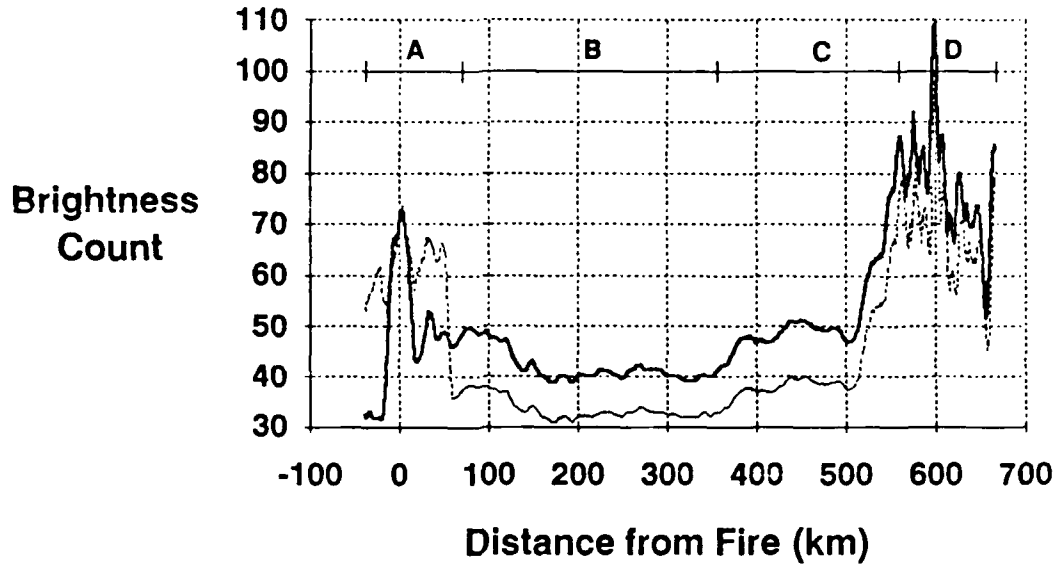


Fig. 4.4. The day 1,  $I_1$  and  $L_2$  values of the length-wise profiles A-D produced for analysis are shown.

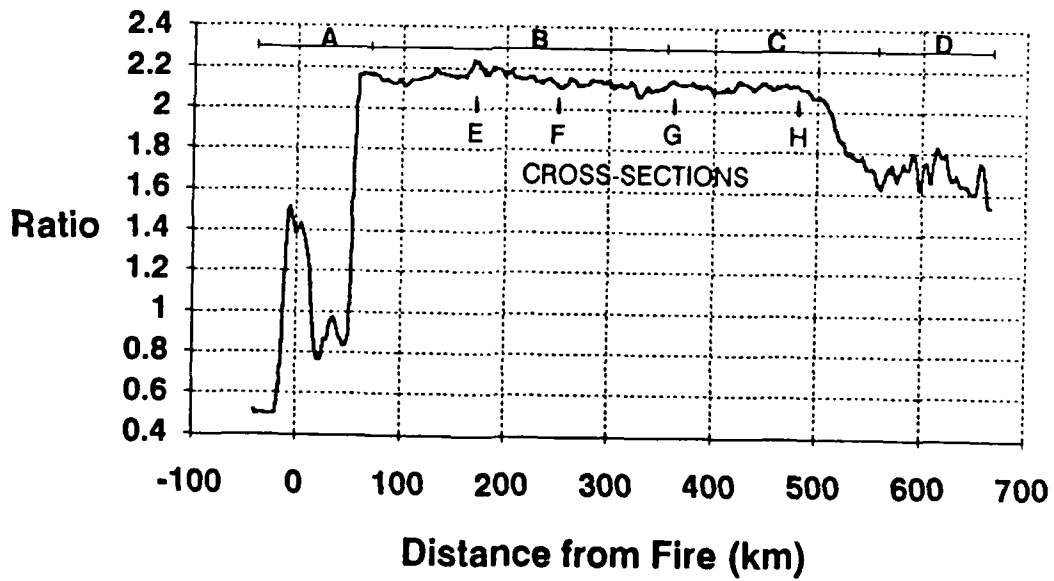


Fig. 4.5. The day 1,  $S_{12}$  lengthwise profiles A-D produced for analysis are shown.

## 1. Smoke Above the Ocean Surface

The significant result to be obtained from Figs. 4.4 and 4.5 is the gradual decrease in  $S_{12}$  from the end of profile segment A until the relatively sharp drop-off at the 500 km point. The smoke particles move between the zero point and the drop off at a speed of 13 knots based on synoptic charts and the Medford, OR sounding. It would take approximately 20 hours for the smoke particles to traverse this distance. Over the 20 hours there is a decrease in  $S_{12}$  value from 2.23 in segment B to 2.08 just prior to the break in segment C. This represents a decrease in  $S_{12}$  of approximately 7 %. The profiles are marked by mesoscale features between the coast crossing at 70 km and the break, but a gradual downward trend persists. The mesoscale features in the profiles may be produced by the mechanisms discussed in Chapter II or by the natural variability of the forest fire output. There is one noteworthy point in the overall trend. Between the point where the smoke crosses from land to water at 70 km and a peak at 180 km there is a gradual  $S_{12}$  increase. The profiles in  $L_1$  and  $L_2$  indicate that there is an initial rise in both values followed by a drop. The slopes of the  $L_1$  and  $L_2$  changes seem to indicate that initially the increase in  $S_{12}$  is caused by gas-to-particle conversion between 70 and 85 km followed by coagulation and sedimentation.

From about 180 km to the break at 500 km a similar analysis of the  $L_1$  and  $L_2$  slopes in conjunction with  $S_{12}$  values indicates that coagulation of the smoke particles is the dominant influence for change. Between the 340 km and 500 km distances  $L_1$  and  $L_2$  both rise and  $S_{12}$  levels off. The smoke in this area is 12-20 hours old if it originated from the OR fire and approximately 9-15 hours old if it originated from the CA fire. The satellite pass was at 1510 local time which would indicate a probability that this is nighttime generated smoke.

If that is the case the smoke would be expected to contain fewer large particles and have a higher  $S_{12}$ .

## 2. Smoke and Surface Radiance Changes

At the 500 km point an accelerated particle size distribution change begins. A drop from 2.08 to 1.77 takes place over the short span of 50 km. This drop is due to one of two possible occurrences.

The smoke is encroaching on the northern edge of the stratus layer. In this visually clear area there is an increase in relative humidity that was analyzed by combining other AVHRR channels. The higher relative humidity of this region lies beneath the smoke plume and is separated from the smoke. However, the marine aerosol mixture made up of nearly saturated particles radiates more equally in both channels. This radiance is seen by the satellite through the optically thin smoke and it lowers the  $S_{12}$  ratio.

The second possible reason for this drop is the radiance from the ocean surface. Other channels of the AVHRR show that the northern portion of the plume lies above colder surface temperatures. The radiance of this colder water may be higher in channel 1 than in channel 2. The satellite may be unduly influenced by the surface, artificially raising  $S_{12}$ . Typically, along the California coast, colder water is upwelled and is richer in nutrients and plankton. The turbidity of this coastal water might also increase channel 1 radiance relative to channel 2 with the same artificial increase in  $S_{12}$ . In either case there is a distinct transition from cold to warm water which occurs at the 500 km point in the profile and the assumption that  $L_w$  is negligible north of the transition is suspect.

### 3. Smoke Interactions with the Stratus Deck

Once the plume is actually over the cloud layer there is a radical change in the  $L_1$ ,  $L_2$  and  $S_{12}$  profiles. Attention should be focused on section D in Figs. 4.4 and 4.5. It is apparent that the profiles have become extremely noisy in the region of the cloud layer. The peaks in  $L_1$  and  $L_2$  and the peaks in  $S_{12}$  are negatively correlated. The spikes in  $L_1$  and  $L_2$  indicate cloud contamination and correspond to the valleys in  $S_{12}$ . In between the clouds are low values in  $L_1$  and  $L_2$  which more nearly reflect the smoke content in those pixels. The analysis of relative humidity distribution indicates the area within the cloud structure is higher in relative humidity than the area to the north. The cloud bank  $S_{12}$  values are uniformly between 1.55 and 1.60. The authentic smoke  $S_{12}$  values should probably be somewhere between 1.90 and 1.75 considering humidity and water influences. The information gained is of little value to the study of the aging process due to the uncertainty of the values.

#### C. CROSS-PLUME ANALYSIS

Four cross-stream profiles were drawn starting at the offshore edge of the smoke plume. They were produced to ensure that the length wise plume profile accurately reflected the metamorphosis of the particle size distributions. By ensuring that the areas of greatest optical depth were periodically examined it is possible to cross check the values of the ratios.

The cross-plume profiles are contained in Figs. 4.6 and 4.7. The left edges of the graphic are aligned at the same vertical pixel column within the image corresponding to the extreme western edge of the southernmost profile. The  $L_2$  spikes on the right of profiles E and G reflect background radiance from land. The maximum radiance in  $L_1$  and  $L_2$  can be tracked right-to-left as the plume

drifts southwest off the coast. The  $L_1$  and  $L_2$  values associated with the maximum radiance decrease until profile H in Fig. 4.6. The increase in  $L_1$  and  $L_2$  in profile H is expected in light of the diurnal variability of the smoke plume. Profile H is in the region that may contain nighttime smoke. The gradual decrease in the radiance and therefore optical depths corresponds to expected coagulation of the smoke plume. The increase in the optical depth in profile H is most likely caused by the increased relative humidity occurring in association with the leading edge of the low lying stratus layer or less turbid water beneath the smoke plume. The influence of this increase in radiance correlates with the lower end of the along-stream profile in Figs. 4.4 and 4.5. The sharp drop in  $S_{12}$  is due to the larger denominator in the ratio.

The similarity in the peak ratio values in Fig. 4.7 confirms the earlier profile in Figs. 4.4 and 4.5. The overall average of the cross-plume values rises slightly from 2.11 at E to 2.14 at F, decreases to 2.12 at G and then drops to 2.03 at H.

#### **D. 18 SEPTEMBER, OVER WATER ANALYSIS**

The change in the synoptic situation between day 1 and day 2 has significant impact. The degree of certainty that was used to assign age to the smoke in the plume has decreased. In addition, the smoke plume on the second day is partially occluded by the continued advance of the low cloud deck from the south. Fig. 4.8 shows the processed  $S_{12}$  satellite image of the plume and the profiles that were drawn for 18 September. The profiles are not nearly as well placed as on day 1 to relate spatial variabilities to temporal variabilities. The plume is just visible along the western edge of the cloud bank in an area that may be affected by underlying humidity. The areas of extreme brightness shown

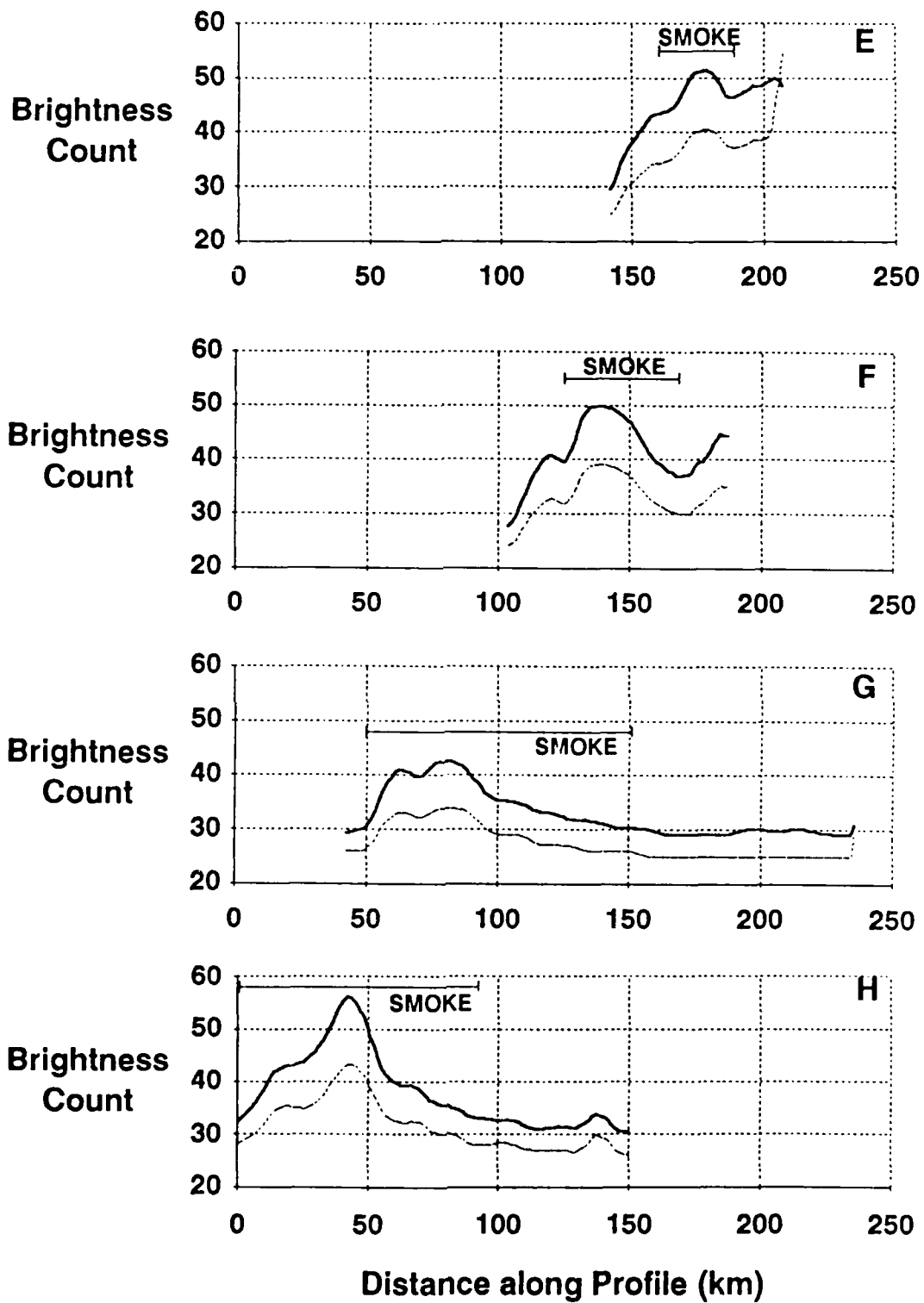


Fig. 4.6. The day 1,  $L_1$  and  $L_2$  profiles E-H produced for analysis are shown.

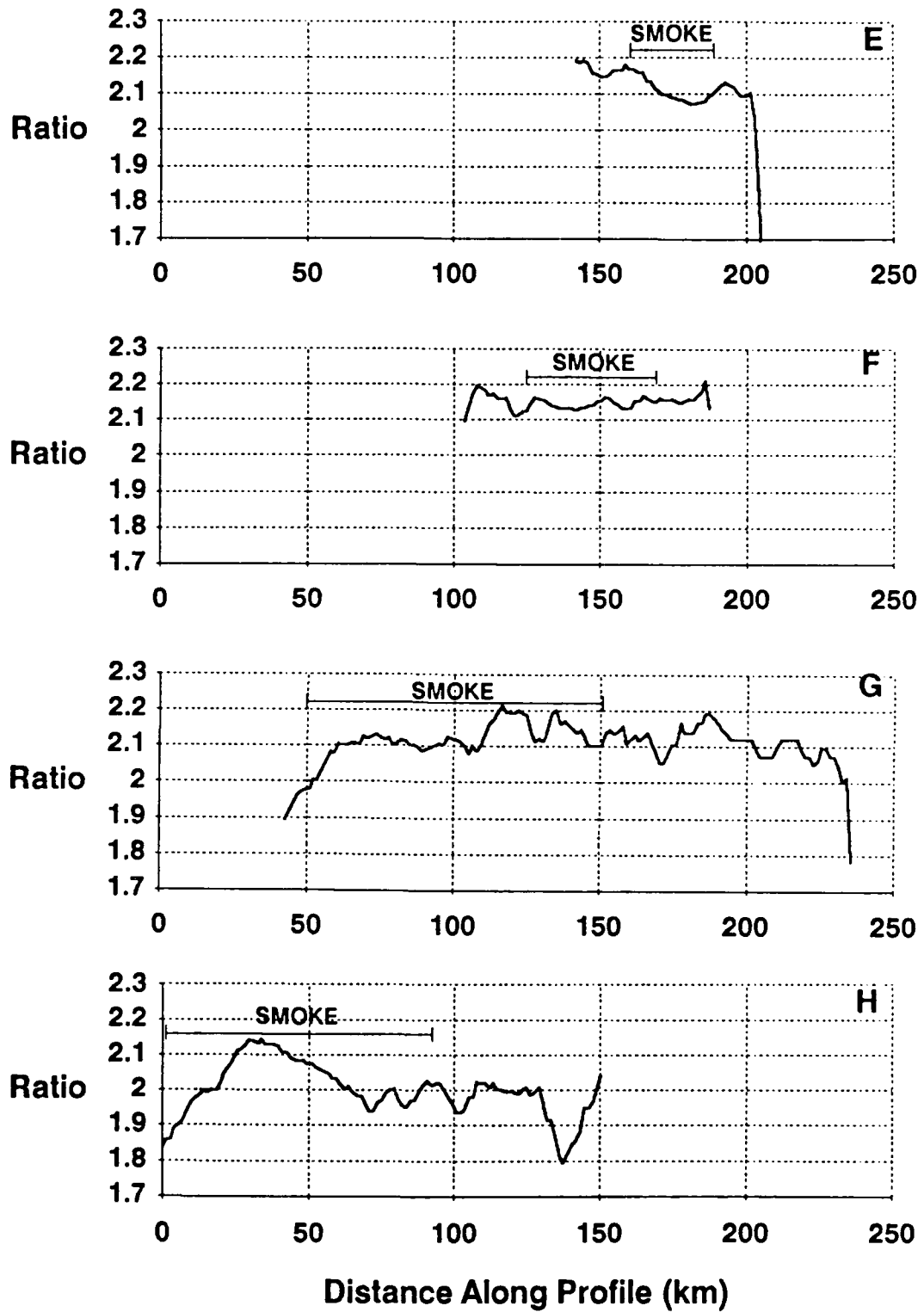


Fig. 4.7. The day 1,  $S_{12}$  cross-plume profiles E-H produced for analysis are shown.



at the south end of profile A and again between B and C are possibly caused by ocean turbidity showing through the smoke. As previously discussed this could affect channel 1 more than channel 2, creating artificially high  $S_{12}$  values.

The hypothesis that turbidity causes the  $S_{12}$  increase in this area is supported by the deviations in  $L_1$  and  $L_2$  at the southern end of profile A in Fig. 4.9. The  $L_1$  increase and the simultaneous  $L_2$  decrease are driven by the above mechanism. This also shows up in Fig. 4.10 as a sharp increase in  $S_{12}$  values. The overall downward trend in Fig. 4.10 is more noticeable than on the previous day. The  $S_{12}$  ratio decreases over the length of the plume from 2.29 to 1.75. The sharp increase at the beginning of profile C is due to interference from land when  $L_2$  is more dominant. Analysis of each profile reveals that each segment has an initial rise in  $S_{12}$  followed by a decline. Fig. 4.9 seems to confirm that there is an initial gas-to-particle conversion region just off shore where  $L_1$  rises faster than  $L_2$ . This is followed by a decrease in  $L_1$ , dropping faster than  $L_2$ , indicating possible coagulation and sedimentation. Profile B has a small segment where  $L_1$  rises rather sharply off a point of land. As in the first segment and as discussed previously, this is possibly a result of turbidity. It might also represent an area of moderate gas-to-particle conversion.

The third segment likewise shows a rise in  $S_{12}$  immediately offshore (Fig. 4.10), but closer examination of  $L_1$  and  $L_2$  in Fig. 4.9 shows that both values are decreasing at a substantial rate. This is most likely an area of coagulation and sedimentation. Beyond 220 km from the fire this profile shows  $L_1$  decreasing faster than  $L_2$  due to coagulation.

The last profile shows the lowest ratios of the over water portion of the study. Here  $L_1$  and  $L_2$  are nearly parallel but moving gradually closer together



Fig. 4.8. Color Enhanced  $S_{12}$  Image, 2259 UTC 18 September 1987: The locations of profiles A-D drawn for analysis are shown.

as  $L_2$  holds steady or rises slightly. Any mesoscale variations are probably due to variations in the output of the fires or in the background radiance beneath the smoke. The characteristics of this area duplicate those of the area below the 500 km point on day 1. The relative humidity below the smoke is significantly higher.

A comparison between day 1 and day 2 indicates that the ratio on day 1 changed about 7% but that the ratio changed by about 28% on day 2. The ratio analysis would seem to indicate much more aging on day 2.

There are four possible explanations for the differences shown by the comparison. The first possibility is that the smoke was transported offshore on 17 September and was "stranded" by a changing synoptic situation. The smoke visible in the satellite image is possibly much older than the travel time estimates. The second possibility is that varying output from the fire changed the characteristics of the smoke. The third possibility is that the mechanisms that age the smoke were changed. The fourth possibility is that there is a higher relative humidity region located in the marine boundary layer underneath the smoke plume. The situation is similar to that of day 1. The higher relative humidity would increase the scattering and therefore the radiance in both channels and equalize  $S_{12}$  values as seen by the satellite.

The synoptic analysis of section IV.A. points most strongly toward the first and the fourth possibilities. It appears that the synoptic situation changed between the satellite passes. However, analysis of the smoke over the land gives evidence to support the other hypotheses and a combination of the effects is probably what is observed. Over-land analysis shows that the CA fire on day 2 was more vigorous and producing larger quantities of smoke with a higher EC

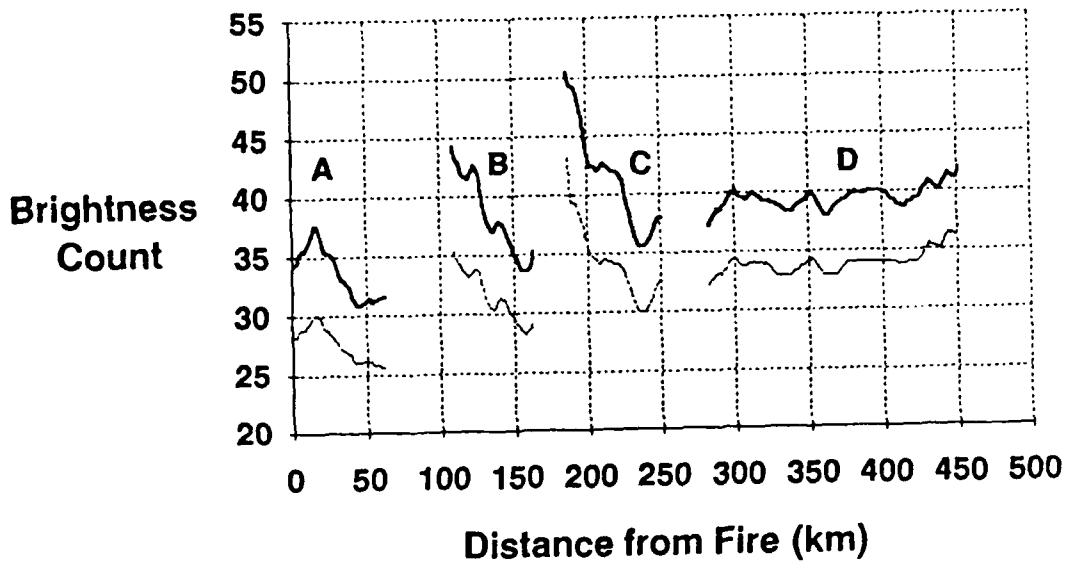


Fig. 4.9. The day 2,  $L_1$  and  $L_2$  profiles produced for analysis are shown.

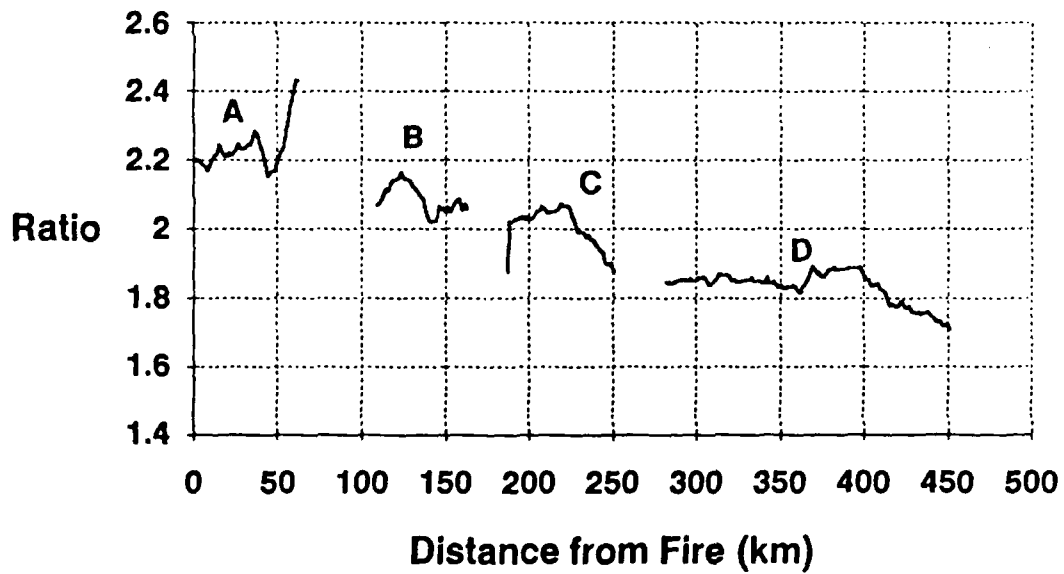


Fig. 4.10. The day 2,  $S_{12}$  profiles produced for analysis are shown.

content. Porch et al. (1986) showed that turbulent energy, such as found in a vigorous fire, contributed to an accelerated coagulation rate. Fires with dense turbulent smoke produced more collisions between particles and had more coagulation. In addition, smoke produced in the presence of flaming combustion should have a lower initial  $S_{12}$  ratio because of the mechanical addition of larger particles to the plume. The increase rate of coagulation and the lower initial value might have an influence on the day 2 data. However, the smoke variation and synoptic changes have minor impact on the satellite observed  $S_{12}$  when compared to the relative humidity change in the area beneath the smoke.

The major influence on the day 2  $S_{12}$  values is probably the increased radiance due to humidity. In the northern portions of the plume that are well away from the cloud layer the  $S_{12}$  values nearly duplicate those of day 1. Where the smoke is visible in the vicinity of the low lying stratus deck the  $S_{12}$  values duplicate those of the southern segments of the day 1 profile. It is concluded that the relative humidity under the smoke caused nearly all of the  $S_{12}$  value modification. This conclusion is supported by the University of Washington data examined in section IV.F.

#### **E. ANALYSIS OF THE SMOKE OVER LAND**

The analysis of the smoke plume over land is based on the profiles shown in Fig. 4.11 that were drawn in the same location for both days. Only those profiles (B and D) best representing the smoke generation process are displayed in Figs. 4.12 and 4.13. In addition to the profiles, color enhanced images are included to show the horizontal dispersion of the particle size distributions. (Figs. 4.14 and 4.15).

Because the background radiances are dependent on many factors it is difficult to obtain spatially detailed information. The subtraction process used to create the  $L_1$  and  $L_2$  images causes degeneration of such detail. In addition, removing the background radiance from under the variations in smoke optical depth removes an unknown quantity of radiance. This is because the radiance upward from the surface depends on the radiation reaching the surface and then passing through the smoke plume a second time. The overall effect of this process would be to eliminate more of the channel 2 radiance than necessary under the optically thin smoke and create an artificially high channel 1:2 ratio.

From Porch et al, (1986) the plume immediately over the fire should contain large particles which are the product of mechanical combustion occurrences and the scouring of the forest floor by firestorm winds. We would expect that the particle size distribution would produce more equal values of  $L_1$  and  $L_2$  immediately over the fire and that as the smoke approached the edge of the plume the heavy particles would begin to settle out. The values of  $S_{12}$  should rise rapidly once the smoke clears the "chimney" of the firestorm.

The profiles drawn through the firestorms of the OR and CA fires are displayed in Figs. 4.12 and 4.13. Of the four profiles produced, only one profile from each day for each fire is shown. Comparison of the lines within each profile shows that the ratio values are approximately 2.0 in the areas of densest smoke. Between pixels 40 and 75 in Fig. 4.12 the fire enlargement on day 2 is indicated by greater spread of lower values. The spiked areas between 0 and 10 and again between 20 and 40 are caused by the background removal process. Fig. 4.13 has regions similar to Fig. 4.12, however the enlargement of the CA fire is clearly visible from pixels 50 to 170. The findings here are supportive of the initial values of the ratio immediately offshore of day 1 of the study.

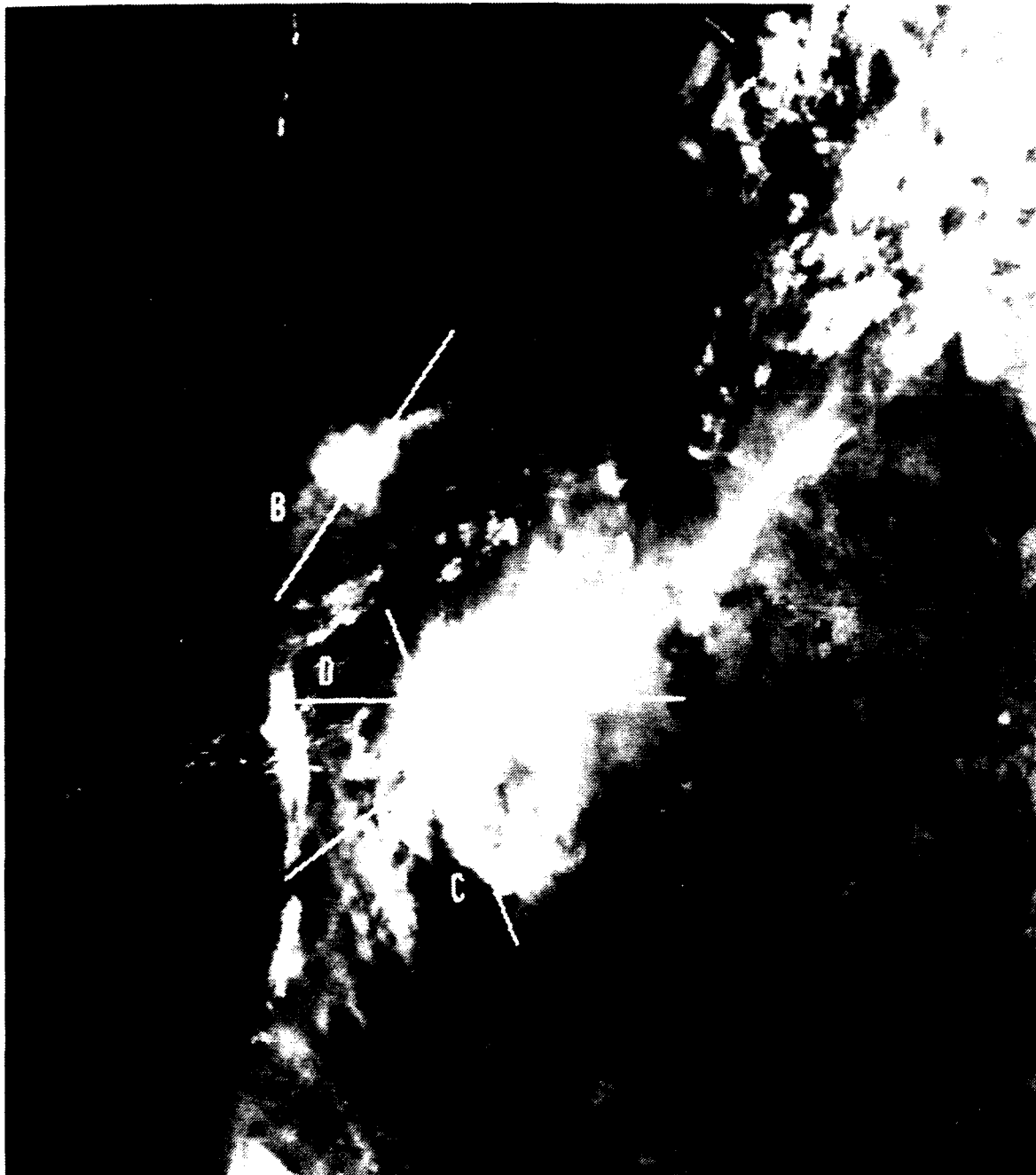


**Fig. 4.11. Channel 1 AVHRR Image, 18 September 1987: The locations of profiles A-D drawn through the CA and OR fires are shown.**

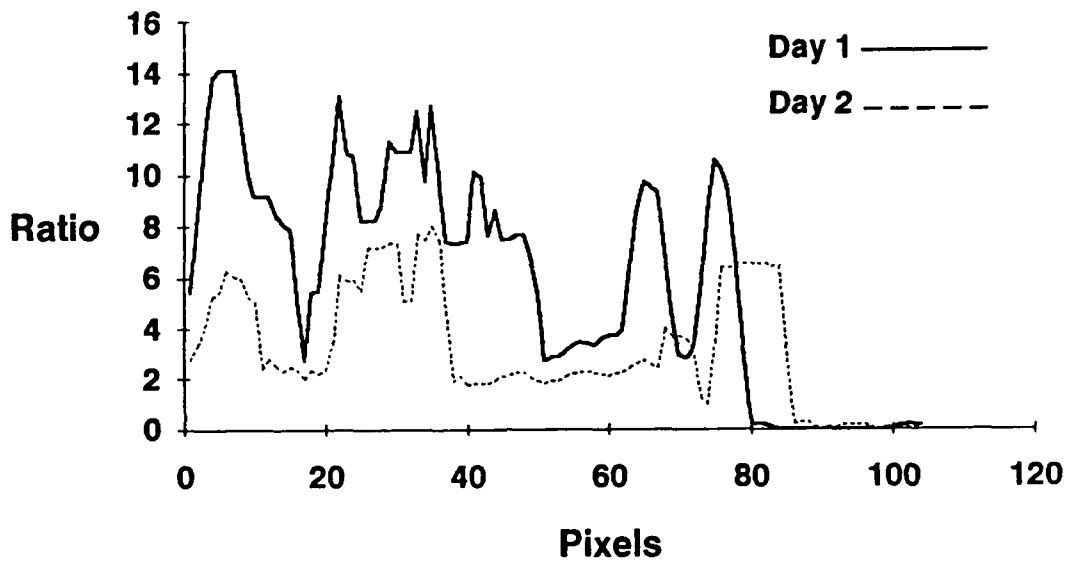


Fig. 4.12. The SW-NE profile (B) of the OR fire comparing the  $L_1/L_2$  ratios of day 1 to day 2 is depicted.

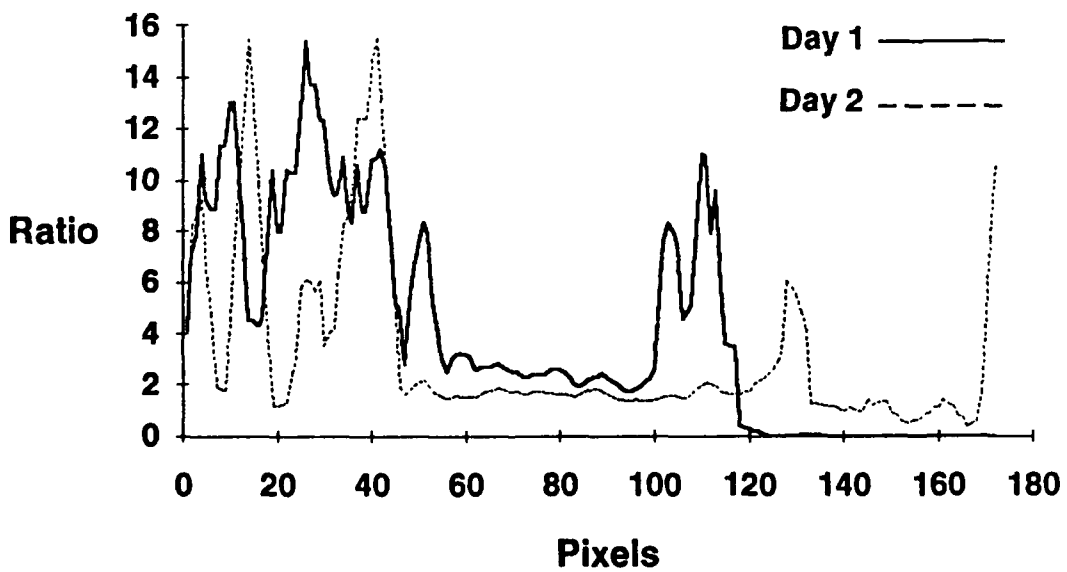


Fig. 4.13. The W-E profile (D) of the CA fire comparing the  $L_1/L_2$  ratios of day 1 to day 2 is depicted.



Both profiles highlight the numerical extent of the  $S_{12}$  variations across the plume. In order to depict the horizontal variations, enhanced images were colored corresponding to the ratio values. These images are shown in Fig. 4.14 and 4.15. The color bar in each image relates color to ratio.

The results obtained through the profiles agree with the smoke aging theory espoused by Porch et al, (1986). As Fig. 4.11 depicts, the  $S_{12}$  ratio over the center of the fire was nearly 2.0. As the profiles traversed the plume these values increase outward from the center.

Once the smoke becomes optically thin the process used to produce the image exerts a large influence on the ratio. Because channel 2 is more responsive to background, when the clear image is subtracted from the smoky image more channel 2 radiance is removed. Therefore, the image depicting the final ratio is artificially high in areas of optically thin smoke. In Figs. 4.12 and 4.13 the area between the individual fire plumes and the coast fits the above described situation. It is unlikely, in light of previous analysis that the  $L_1/L_2$  ratio exceeds 3.0 at any point. However, in the color images areas approach values of 6.0 or higher. Further research into the removal of background effects over land is warranted.

The smoke plume on day 2 shows that some synoptic changes have occurred. During day 1 the smoke was limited in its northern travel by terrain and the natural tendency for smoke to "flow" downhill (Porch et al, 1989). The smoke traveled to the SSW in a narrow vertical band estimated to be between 1200 and 1500 meters. During day 2 the smoke showed a tendency to drift ENE emulating the upper level cirrus band in Figs. 4.11 and 4.15. This tendency indicated smoke was transported higher into the atmosphere by the more active burning visible in the profiles and the color imagery. This conclusion is



**Fig. 4.14. Color Enhanced  $L_1/L_2$  Image on day 1: The smoke plume over land is shown.**



**Fig. 4.15. Color Enhanced  $L_1/L_2$  Image on day 2: The smoke plume over land is shown.**

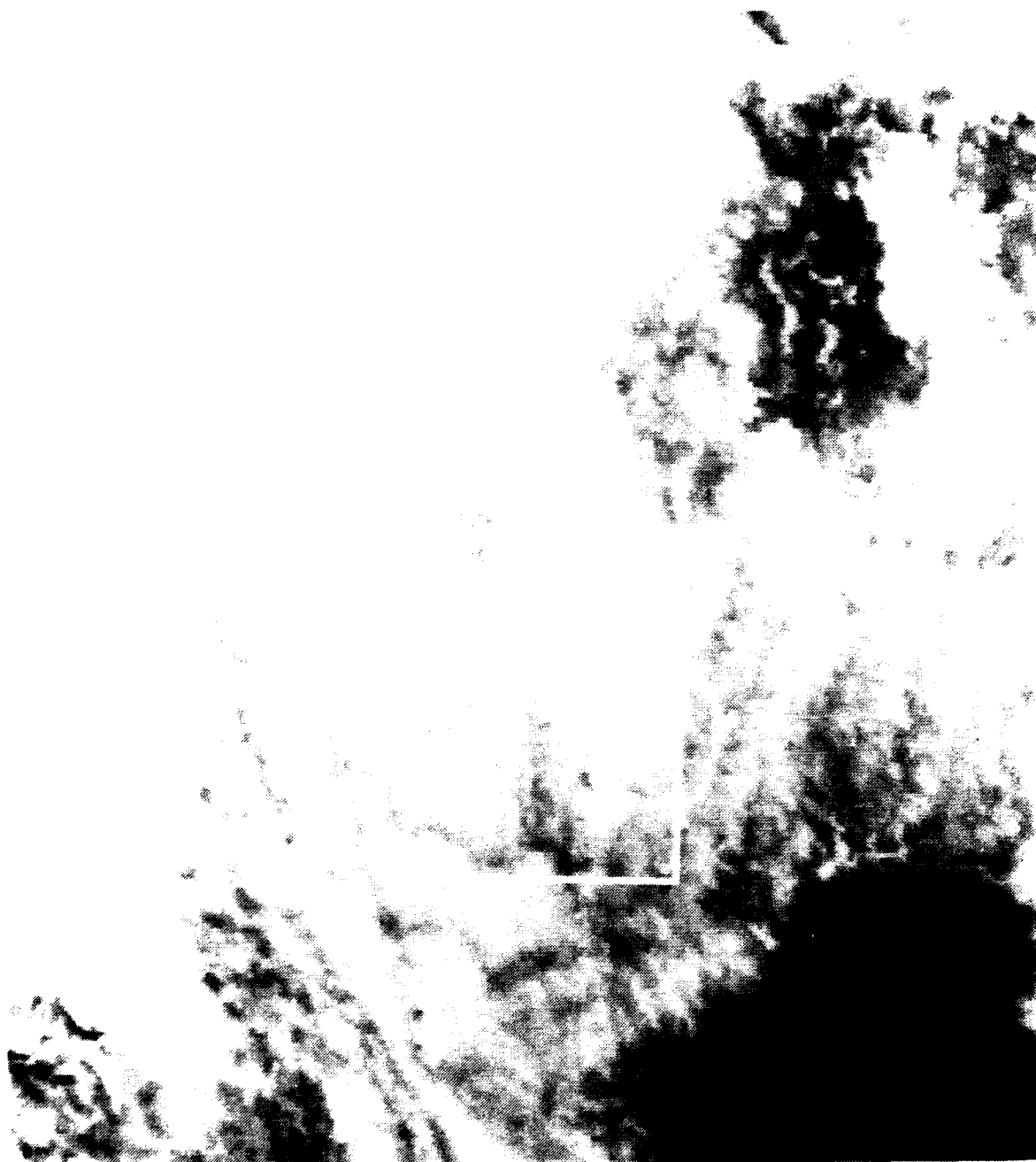


**Fig. 4.16. Channel 4 AVHRR Enlarged Image taken of day 1:  
Within the box are several darker hot spots of active combustion.**

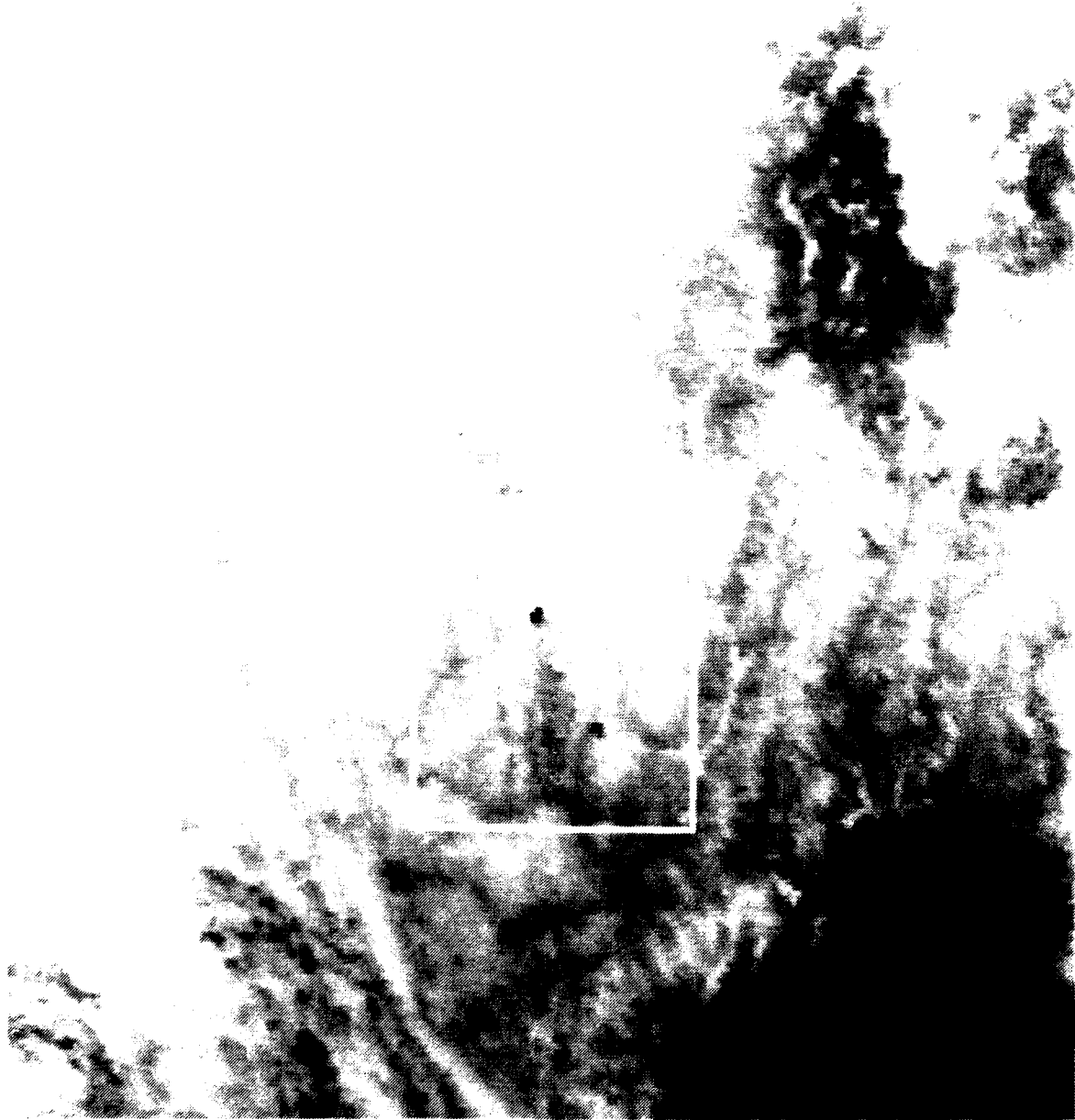


**Fig. 4.17. Channel 4 AVHRR Image taken on day 2: Within the box are more intense and more numerous hot spots than on day 1.**

supported by imagery in channel 4 showing more numerous hot spots generated by the combustion on day 2 (Figs. 4.16 and 4.17). Fig. 4.15 shows the bulk of the plume drifting ENE and extensive areas of lower ratios. The drift to the ENE is the product of the slightly altered synoptic picture that produced light westerly winds above 700 mb.

#### **F. UNIVERSITY OF WASHINGTON FINDINGS**

The University of Washington flew their C-131F aircraft into the smoke plume as identified by the satellite imagery. Aircraft instrumentation included grab-bag sampling of the gases and continuous readouts on the extinction, scattering and absorption coefficients. They were able to pursue the smoke further to the south and take samples at ranges of over 1000 km from the fire. Their data confirmed separation between the cloud layer and the smoke and estimated smoke altitude.

Fig. 4.18 is a depiction of the particle size distribution curves corresponding to samples taken at the firehead and at 25 and 44 hours. As shown, the slope of the right side of the distribution curves flatten with age. This strongly agrees with the results of the satellite analysis of the smoke plume. The rate of change between the firehead and 44 hours closely approximates the rate of change over day 1. The day 2 changes are not germane. Fig. 4.19 shows how the particles within the accumulation mode grew over the time period of the study.

Two important conclusions can be drawn from this figure. The first is that particles with similar light scattering coefficients grew at rates associated with the concentration of the smoke. All samples taken over the fire were

characterized by their light scattering coefficient due to dry particles. The samples were analyzed for mean particle diameter. As samples were taken over the period of the study, the light scattering coefficient,  $\sigma_{sp}$  and the mean particle diameter were plotted. The particles generally increased in diameter with the passage of time. Those with smaller light scattering coefficients that are proportional to the mass concentration of the particles grew at a faster rate. This is attributed to increased coagulation rates in areas of heavier smoke concentrations. The more light scattering particles grew at a slower pace and were the only ones still present in the plume at the end of the 44 hour period. The particles represented by the asterisks in Fig. 4.19 are of particular interest. These particles grew in size from 0.32 to 0.34  $\mu\text{m}$  over the 44 hours included in the study. This growth rate is about 6 % over 44 hours or about 3 % over the approximately 20 hours of the day 1 smoke travel. A 3 % drop would produce a  $S_{12}$  ratio change from 2.14 to about 2.08. That is the drop that occurred on 17 September across the area of the plume from the coastal crossing to the 500 km break. This verifies the conclusion that relative humidity affected the area below the 500 km point on day 1 and nearly all observations on day 2.

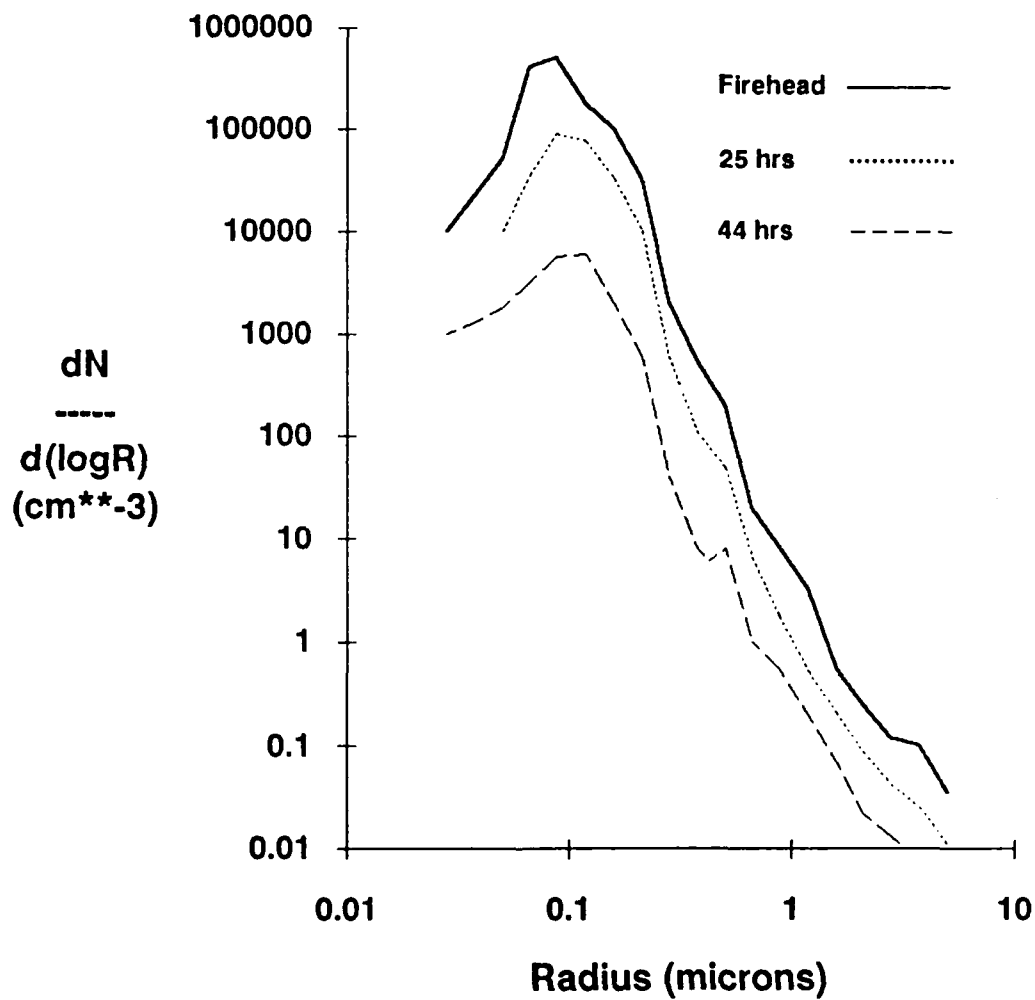


**Fig. 4.18. A comparison of the initial size distribution curve with that of 44 hours. This demonstrates the size distribution changes that take place during the aging process (University of Washington data).**



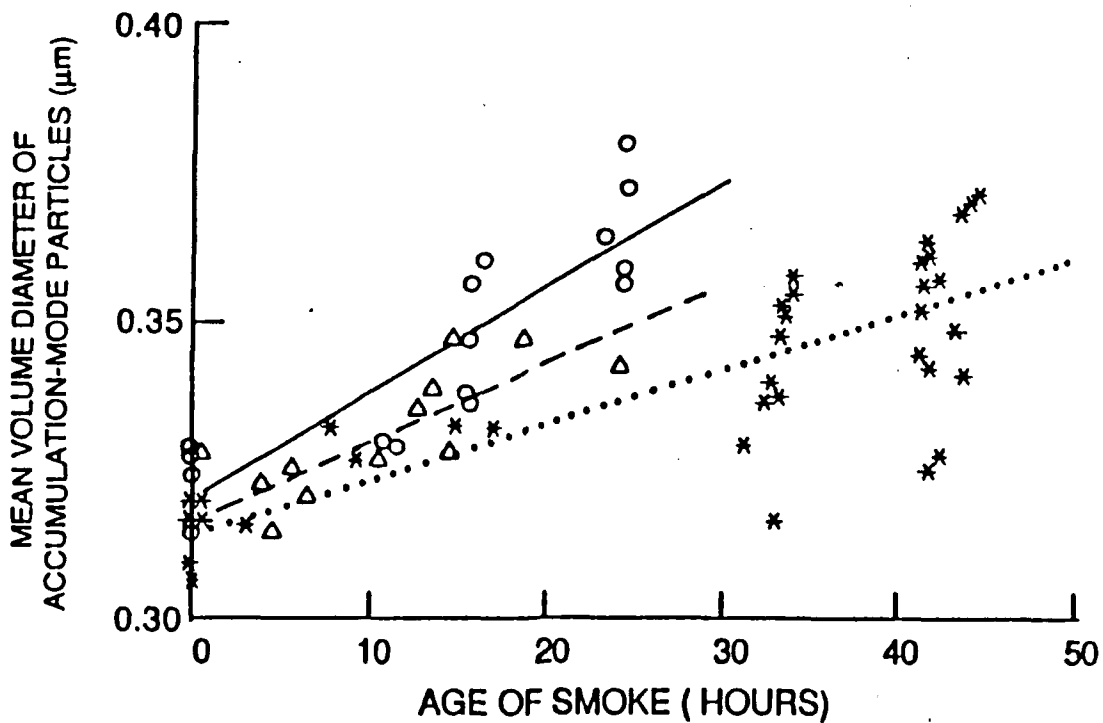


Fig. 4.19. Accumulation Mode Particle Size Growth: The particle size changes are depicted for the period of the U. of W. study. The geometric volume diameter of the particles in the accumulation mode is plotted against the age of the smoke. The measurements are differentiated by the value of the light scattering coefficient due to dry particles ( $\sigma_{sp}$ ). The circles and solid line are associated with a  $\sigma_{sp}$  between  $2.0 \times 10^{-2}$  and  $5.0 \times 10^{-4}$ , the triangles and dashed line with  $\sigma_{sp}$  between  $5.0 \times 10^{-4}$  and  $1.0 \times 10^{-5}$  and the stars and dotted line with  $\sigma_{sp}$  larger than  $10^{-3}$ .

## V. CONCLUSIONS AND RECOMMENDATIONS

Satellite data from NOAA-9 AVHRR were used to analyze forest fire smoke over the eastern North Pacific and coastal mountains. Channel 1 and Channel 2 data were used to compile images and profile the particle size distribution of the smoke in both of the above regions. The results of the study are:

1. Smoke may be usefully depicted using combined channel 1/channel 2 imagery.
2. The smoke undergoes an aging process that may be analyzed through satellite imagery.
3. The particle size distribution altering mechanisms of coagulation, sedimentation, condensation and gas-to-particle conversion are discernable through satellite imagery.
4. Optically thin smoke allows background influences to affect the  $S_{12}$  ratio both over water and over land introducing some inaccuracies into the ratio.
5. Background influences may be either analyzed by using other channels of the AVHRR or removed through a subtraction process with varying degrees of success.

The conclusions reached from these results are that satellite imagery can be used to effectively trace and determine the age of smoke plumes. Satellite imagery can be used to derive  $S_{12}$  values and determine the slope of the particle size distribution curve. The imagery can provide information relative to the changes in the distribution and the changes can be projected into the future in an effort to predict optical thickness for certain weapons and sensors. The weapons and sensor management for future large scale battle problems could benefit ultimately from continued research in this area.

The technique of subtracting background information in channel 1 and channel 2 from the pollution bearing image and forming a ratio of the remainders is easily accomplished if the images are only a few days apart. When more than a few days have passed, many adjustments are necessary throughout the image to eradicate background effects. Background effects have only minor impact in areas where the smoke optical depths are large, but where smoke is optically thin the pixel-to-pixel variations are too detailed for the subtraction process. The subtraction technique needs improvement that might be achieved by subdividing the two images into smaller areas that are each corrected for sun-satellite geometry and vegetation changes. The smaller the area in the subdivided images the more accurate the subtraction process.

Further refinement also can be achieved using Mie scattering theory to produce tables of expected optical depths for a theoretical or aircraft confirmed smoke mixture. These tables would predict the  $S_{12}$  ratio based on extinction coefficients calculated by Mie scattering theory.  $S_{12}$  observed by the satellite would reflect deviations in the particle size distribution from the predicted values. A series of similar look-up tables might allow derivation of a mean particle size. Research should continue in this area and on this forest fire case because the University of Washington aircraft data have provided 'ground truth' and a reliable mean particle size.

More research also needs to be done on the rate with which the aging process takes place. The rate of aging through coagulation and sedimentation is most dependent on the concentration of the smoke particles. Well diluted smoke has a marked decrease in particle collisions. With fewer collisions the aging process becomes very slow and the smoke can remain airborne for extended periods.

As mentioned above, there is a large amount of further study and research that can be done with these data. The occurrence of a fire of this magnitude offering three varying and cleanly separated environments for study is a rare opportunity to gain further understanding of smoke's life cycle in the atmosphere. Understanding the variables that affect smoke's contribution to solar energy reduction should promote a better understanding of the nuclear winter phenomenon.

## LIST OF REFERENCES

- Angell, J.K., and J. Korshover, 1985: Surface temperature changes following the six major volcanic episodes between 1780 and 1980. *J. Appl. Meteor*, **24**, 937-951.
- Alvarez, L. W., W. Alvarez, F. Asaro, and H. W. Michael, 1980: Extraterrestrial cause for the Cretaceous-Tertiary extinction. *Science*, **208**, 1095-1108.
- Chung, Y. S., and H. V. Le, 1984: Detection of forest-fire smoke plumes by satellite imagery. *Atmos. Envir.*, **18**, 2143-2151.
- Crutzen, P. J., and J. Birks, 1982: The atmosphere after a nuclear war: twilight at noon. *Ambio*, **11**, 114-125.
- Crutzen, P. J., I. E. Galbally and C. Bruhl, 1984: Atmospheric effects of post-nuclear fires. *Climatic Change*, **6**, 323-364.
- Durkee, P. A., 1984: The Relationship Between Marine Aerosol Particles and Satellite-Detected Radiance. Ph.D. Thesis, Colorado State University, Ft. Collins, CO, 124 pp.
- Fosberg, M. A. and H. Record, 1980: Emissions and air resource management within forests. Presented at the Symposium on Effects of Air Pollutants on Mediterranean and Temperate Forest Ecosystems, Riverside, California, June 22-27, 1980.
- Friedlander, S. K., 1965: The similarity theory of the particle size distribution of the atmospheric aerosol. In *Aerosol - Physical Chemistry and Application*, (edited by K. Spurny), Gordon and Breach.
- Friedlander, S. K., 1977: *Smoke, Dust and Haze*. John Wiley & Sons, Inc., 317 pp.
- Frost, E. M., 1988: Global Scale Estimates of Aerosol Particle Characteristics. Master's Thesis, Naval Postgraduate School, Monterey, California, 46 pp.
- Fuchs, N. A., 1964: *The Mechanics of Aerosols*. Pergamon Press, 298 pp.
- Gordon, H. R., 1978: Removal of atmospheric effects from satellite imagery of the oceans. *Appl. Opt.*, **17**, 1631-1636.
- Hanel, G., 1976: The properties of atmospheric aerosol particles as functions of the relative humidity at thermodynamic equilibrium with the surrounding moist air. In *Advances in Geophysics*, **19**, 73-178. Edited by H. E. Landsberg and J. Van Mieghen, Academic Press.
- Kidwell, K.B., 1986: NOAA Polar Orbiter Data Users Guide, U. S. Department of Commerce, December 1986.

- Kaufman, Y. J., R. S. Fraser and R. H. Farrare, 1988: Satellite measurements of large scale air pollution - method. unpublished paper dated 11 April, 1988.
- Kaufman, Y. J. and J. H. Joseph, 1982: Determination of surface albedos and aerosol extinction characteristics from satellite imagery. *J. Geophys. Res.*, **87**, 1287-1299.
- Palmer, T., 1981: Large fire winds, gases and smoke. *Atmos. Envir.*, **15**, 2079-2090.
- Pittock, A. B., T. P. Ackerman, P. J. Crutzen, M. C. MacCracken, C. S. Shapiro, and R. P. Turco, 1986: *Environmental Consequences of Nuclear War*. John Wiley and Sons, pp. 359. Edited by R. E. Munn.
- Porch, W. M., J. E. Penner and D. A. Gillette, 1986: Parametric study of wind generated super- $\mu\text{m}$  particle effects in large fires. *Atmos. Envir.*, **20**, 919-929.
- Porch, W. M., S. Barr, W. E. Clemmets, J. A. Archuleta, A. B. Fernandez, C. W. King, W. D. Neff, and R. F. Mosker, 1989: Smoke flow visualization in a tributary of a deep valley. *Bull. Amer. Meteor. Soc.*, **70**, 30-35.
- Radke, L. F. J. L. Stith, D. A. Hegg, and P. V. Hobbs, 1978: Airborne studies of particulate gases from forest fires. *J. Air Poll. Control Assoc.*, **28**, 30-34.
- Radke, L. F., A. S. Ackerman, J. H. Lyons, D. A. Hegg, P. V. Hobbs, J. E. Penner, and R. E. Weiss, 1989: Effects of aging on the smoke from a forest fire: Implications for the nuclear winter hypothesis. Unpublished article prepared for the *J. Geophys. Res.* 22 pp.
- Rahn, K. A., C. Brosset, B. Ottar, and E. M. Patterson, 1982: Black and white episodes: Chemical evolution of Eurasian air masses and long-range transport of carbon to the Arctic. In *Particulate Carbon: Atmospheric Life Cycle* (G. T. Wolff and R. L. Klimisch, Eds.), Plenum Press, pp 327-342.
- Ramsey, R. C., 1968: Study of the Remote Measurement of Ocean Color. Final Report, TRW, NASW-1658.
- Shettle, E.D. and R.W. Fenn, 1979: Models for aerosols of the lower atmosphere and the effects of humidity variations on their optical properties. AFGL-TR-79-0214 Air Force Geophysics Laboratories, Hanscom AFB, MA, 94 pp.
- Stiles, D. C., 1983: Evaluation of an  $\text{S}_2$  sampler for receptor modeling of woodsmoke emission. Paper No. 83-54.6, Annual Meeting of Air Pollution Control Association, 19-24 June, 1983.
- Turco, R. P., O. B. Toon, T. P. Ackerman, J. B. Pollack, C. Sagan, 1983: Nuclear winter: Global consequences of multiple nuclear explosions. *Science*, **222**, 1283-1292.

- van de Hulst, H. C., 1957: *Light Scattering by Small Particles*. John Wiley & Sons, Inc., pp. 469.
- Waggoner, A. P., R. E. Weiss, N. C. Ahlquist, D. S. Covert, S. Will, R. J. Charlson, 1981: Optical characteristics of atmospheric aerosols. *Atmos. Envir.*, **15**, 1891-1909.
- Wallace D., and R. Chaun, 1976: A cascade impaction instrument using quartz crystal microbalance sensing elements for 'real time' particle size distribution studies. Presented at the 8th Materials Research Symposium, September 1976, pp. 24-25.
- Wexler, H., 1950, The great smoke pall: September 24-30, 1950. *Weatherwise*, **3**, 6-11.
- Wolff, G. T., 1985: Characteristics and consequences of soot in the atmosphere. *Environment International*, **11**, 259-269.

## INITIAL DISTRIBUTION LIST

		Number of Copies
1.	Defense Technical Information Center Cameron Station Alexandria, VA 22304-6145	2
2.	Library, Code 0142 Naval Postgraduate School Monterey, CA 93943-5002	2
3.	Chairman (Code 63Rd) Department of Meteorology Naval Postgraduate School Monterey, CA 93943	1
4.	Chairman (Code 68Co) Department of Oceanography Naval Postgraduate School Monterey, CA 93943	1
5.	Professor P. A. Durkee (Code 63De) Department of Meteorology Naval Postgraduate School Monterey, CA 93943	22
6.	Professor J. A. Nystuen (Code 68Ny) Department of Oceanography Naval Postgraduate School Monterey, CA 93943	1
7.	CDR Peter J. De Vries OinC, NOSC Hawaii Lab PO Box 997 Kailua, HI 96734-0997	2
8.	Director Naval Oceanography Division Naval Observatory 34th and Massachusetts Avenue NW Washington, DC 20390	1
9.	Commander Naval Oceanography Command Stennis Space Center, MS 39529-5000	1



- |     |   |   |
|-----|---|---|
| 10. | Commanding Officer<br>Naval Oceanographic Office<br>Stennis Space Center, MS 39522-5001   | 1 |
| 11. | Commanding Officer<br>Fleet Numerical Oceanography Center<br>Monterey, CA 93943   | 1 |
| 12. | Commanding Officer<br>Naval Ocean Research and Development Activity<br>Stennis Space Center, MS 39529                               | 1 |
| 13. | Commanding Officer<br>Naval Environmental Prediction Research Facility<br>Monterey, CA 93943  | 1 |
| 14. | Chairman Oceanography Department<br>U. S. Naval Academy<br>Annapolis, MD 21402  | 1 |
| 15. | Chief of Naval Research<br>800 N. Quincy Street<br>Arlington, VA 22217  | 1 |
| 16. | Office of Naval Research (Code 420)<br>Naval Ocean Research and Development Activity<br>800 N. Quincy Street<br>Arlington, VA 22217 | 1 |